The Pennsylvania State University

The Graduate School

EFFECTS OF BIOFILM SPATIAL DISTRIBUTION ON THE SETTLING AND TRANSPORT OF MICROPLASTIC PARTICLES

A Thesis in

Mechanical Engineering

by

Annalie E Fazio

Submitted in Partial Fulfillment
of the Requirements
for the Degree of

Master of Science

August 2022

The thesis of Annalie Fazio was reviewed and approved by the following:

Margaret Byron
Assistant Professor of Mechanical Engineering
Thesis Advisor

John M. Regan
Professor of Environmental Engineering

Matthew Rau
Assistant Professor of Mechanical Engineering

Daniel Haworth
Professor of Mechanical Engineering
Chair of the Graduate Program

ABSTRACT

Microplastic (MP) particles-- small pieces of plastic ranging from nanometers to several millimeters in length-- are becoming more and more common in aquatic ecosystems all over the world, and are a major source of pollution within the environment. They enter the environment from many channels and in a variety of forms, including microfibers shed from clothing, microbeads from cosmetics, and a number of byproducts from industrial processes. Upon their introduction into the environment, plastic particles may be inert, but they quickly become active participants within ecosystems due to the growth of biofilms upon their surfaces. These biofilms include microbial communities of bacteria, algae, fungi, protozoa, and other microorganisms, which adhere to virtually all surfaces. The biofilms formed upon the surfaces of MPs affect important physical parameters, such as settling velocity and aggregation potential; however, very little research focuses on how the presence and/or spatial distribution of biofilms over the microplastics' surface can affect their overall transport. Particle-scale physical properties like shape, mass distribution, and surface properties may play a major role in how MPs are transported throughout the environment; biofilm development (and its uniformity or non-uniformity over a surface) affect these properties. Here, we investigate how the presence and the spatial distribution of biofilm affects the settling and rising of MPs. As a starting point, we compare the rising behavior of positively buoyant virgin plastic pellets (nurdles) subjected to two different biofilm colonization regimes. In the first of the two colonization regimes, nurdles float undisturbed at the water surface and biofilm develops only on one side of the plastic. In the second, nurdles are regularly mixed into the water, allowing the biofilm to develop on all sides. The nurdles were then recorded while rising through water, using a macro lens and a high-speed videography. From the videos, we extracted the rising kinematics and calculated the rising velocity; we then compared the rising velocity and overall rising behavior between the differently colonized MPs. We find that the

presence of biofilm reduces rising velocity relative to the un-biofilmed case, and that the non-uniformly biofilmed nurdles rise more slowly than the uniformly biofilmed nurdles despite similar biofilm coverage (in the regions of the nurdles that do have biofilm present). This leads to the conclusion that the spatial distribution of biofilm affects rising velocity, and may be a key factor in the overall environmental transport of MPs.

TABLE OF CONTENTS

LIST OF FIGURES

LIST OF TABLES

ACKNOWLEDGEMENTS

I would like to thank Dr Margaret Byron for all the time and effort she has put into supporting me over the last two years as well as always being there to help me out of some really tough spots during this project. I would also like to thank Dr Jay Regan for being an amazing collaborator, for your great advice, and allowing us to use your equipment to help us out with our project. Additionally, I would also like to thank Dr Matthew Rau and all of my lab mates for always offering their help, support, and great advice.

Finally, I would like to thank all my friends and family members, especially my parents and grandmother, who encouraged me to keep going when times got tough and cheered me on through my whole graduate school experience.

Chapter 1: Introduction

1.1 Background and motivation

The global demand for the production of plastic has increased exponentially over the past six decades. In this modern day and age, industry has discovered that plastic products are significantly cheaper to manufacture than other products like glass, metal, and paper (Andrady, 2011). Plastic is an incredibly versatile product that can be used for several different applications with its strong and lightweight characteristics. Some of these uses include microbeads used in cosmetics and household cleaning products (Dauvergne, 2018), textiles made into fabric or cloth for clothing and other garments (Liu et al., 2021), or as virgin plastic pellets used as a raw material in the production of plastic goods like disposable packaging, water bottles, etc. (Čulin & Bielić, 2016). These plastics are then introduced into aquatic environments through a variety of different pathways such as falling off of cargo ships during transportation, as run-off from processing facilities, or getting washed down the drain after use (Andrady, 2017). Once introduced into the environment, plastic products have the potential to be broken down into even smaller and smaller pieces producing hundreds, if not thousands more individual pieces of plastic to spread throughout the environment to oceans, rivers, and other major bodies of water.

When plastic products are discarded into the environment, they experience different weathering conditions, depending on the environment to which they are exposed. Sources of weathering include (for example) UV radiation (Yousif & Haddad, 2013) and shear stresses due to contact grazing with other sediments in the water (Enfrin et al., 2020). This can cause the breakdown of larger plastic items into smaller particles known as microplastics. A microplastic is defined as any piece of plastic of any shape – for example films, fragments, fibers, spheres, or many

other shapes – that is less than 5 mm in size (Thompson et al., 2004). This plastic waste has been found in all the world's ecosystems, including locations as varied as agricultural soil (Chae & An, 2018), the polar ice caps (Stefánsson et al., 2021), freshwater mountain lakes (Pastorino et al., 2022) and the global ocean (W. C. Li et al., 2016). A major area of interest in the study of microplastic pollution is the behavior of plastics within aquatic systems since they are a major sink for microplastics within the environment. Additionally, the presence of microplastics in these systems is grossly underestimated (Lindeque et al., 2020).

Once microplastics are introduced into the environment, they become part of it – interacting with all the things around them, whether living or non-living. Due to their small size, microplastics are easily ingested by aquatic organisms, which in turn has the potential to negatively impact their health (Y. Li et al., 2021). Moreover, these tiny fragments of plastic can also carry disease-causing organisms, which act as a vector for diseases within the environment (Pham et al., 2021). These disease-causing organisms, along with other microorganisms like bacteria, algae, fungi, and protozoa, attach to the surface of microplastics and form biofilms.

Biofilms are communities of microorganisms (e.g., bacteria, fungi, algae) that exist within moist natural environments and can be either free-floating or attached to a surface. The presence of biofilms on the surface of microplastics can affect important physical parameters like settling velocity (Semcesen & Wells, 2021) and aggregation potential (Lagarde et al., 2016). However, very little is known about how the presence of biofilms affects the overall transport of microplastics. For example, there are few reports on how biofilms affect the longevity of microplastics within aquatic environments – do certain types of bacteria or microorganisms cause specific plastics to degrade? Do they extend the amount of time plastics remain in the environment? We also do not know how biofilm architecture and spatial distribution affect the overall settling and rising behavior of microplastics – how does a non-uniformly distributed biofilm affect the rise

velocity of a microplastic? How do these qualities affect lateral dispersion of microplastics? These are some of the questions we aim to explore.

In this thesis, we present a pilot study on the impact of biofilm spatial distribution on the settling of microplastics and their transport within the environment. Following an overview of the current state of the field, we describe the methods used to colonize virgin plastic particles (nurdles) made of high-density polyethylene (HDPE) with an isolated strain of cyanobacteria (*Anabaena*) under two different colonization regimes – non-uniform (one-sided) growth and uniform (all sides) growth. We then use high speed videography to capture the trajectories of the (positively buoyant) microplastics as they rise through a tall water tank. From the videos of the rising nurdles, we extract parameters of interest such as rise velocity and lateral motion. We then present our results and discuss them in the context of global microplastic transport.

1.2 Literature Review

1.2.1 Introduction of microplastics into the environment

Nurdles are small (~3mm) pieces of plastic that serve as raw material in the production of plastic products. They are made of a variety of materials including polyethylene (PE), polypropylene (PP), polystyrene (PS), polyvinyl chloride (PVC), and other plastics. Nurdles are ground and melted to form finished plastic products. Nurdles themselves and the plastic products they are made into can enter the environment; these are known as primary plastics. When they undergo environmental weathering processes that cause fragmentation into smaller pieces, they create secondary plastics. Microplastics can exist as either primary plastics (from nurdles, microbeads, or other small plastics released directly into the environment) or secondary fragments (weathered fragments of larger items).

Weathering by physical, chemical, and biological processes causes the breakdown of microplastics into smaller particles once they are introduced into the environment (Duan et al., 2021). The physical breakdown of microplastics can be caused by mixing with sand and sediment or brushing up against rocks due to wind- or wave-driven flow. Through these collisions, microplastics experience abrasive and shear forces that induce their fragmentation into smaller pieces (Enfrin et al., 2020). Photodegradation is another process which causes the physical breakdown of larger plastic items into microplastics. Plastic is made up of polymer chains that absorb ultra-violet light when exposed to the sun. Irradiation by UV light excites molecules within the polymer chains, destabilizing bonds and eventually breaking the polymer chains. This leads to the further breakdown of plastic particles (Yousif & Haddad, 2013). Lastly, biological degradation based on microplastics' interactions with organisms present in the environment can break down plastic into smaller pieces. Some studies have shown that ingestion by aquatic organisms can also cause the fragmentation of microplastics (Cau et al., 2020; Dawson et al., 2018). The end result of this breakdown yields microplastics with a wide variety of sizes, shapes, and physical properties. All these factors affect how they are transported in the environment.

When microplastics enter the environment (either primarily or secondarily), they are subject to similar transport processes as those that mobilize other materials present within the water column (Horton & Dixon, 2018). These include gravitational effects based on physical properties (e.g., mass density and particle shape) and also differences in fluid flow in rivers, lakes, and ocean currents (Costa, 2016). Mass density strongly affects the behavior of a microplastic suspended within an aquatic environment. Particles with a density less than or close to that of water will tend to rise towards the surface of the water whereas denser particles tend to sink. However, Kowalski et al. (2016) showed that in some cases, less dense particles can settle at a faster rate than denser ones; this indicates that particle shape also has a strong influence on the settling behavior of microplastics. Since they are transported along with other material within the water column, even

buoyant microplastics have the potential to aggregate with denser particles and sink along with them. This can then result in broad vertical distribution of microplastics, from close to the surface all the way down to be buried in the bottom sediments of the aquatic environment (Pohl et al., 2020).

Aggregation with denser debris is not the only cause for the sinking of typically buoyant microplastics. The density of microplastics can physically change once introduced into the water column due to their tendency to accumulate surface foulants. These foulants include (for example) microalgae and larvae that attach to and grow on the surface of microplastics, increasing their density and causing them to sink deeper into the water column—therefore contributing to the wide range in the vertical distribution of plastic particles in the water column (Amaral-Zettler et al., 2021; Kaiser et al., 2017; Semcesen & Wells, 2021).

1.2.2 Colonization of microplastic particles by microbes

Microplastics, once introduced into the environment, become part of it and begin to interact with all the organisms living within it. Plastic particles become a new surface upon which biofilms can form. Biofilms are intricate communities of microorganisms composed of bacteria (Kostakioti et al., 2013), algae (Thapa et al., 2017), protozoa (Arndt et al., 2003), and fungi (Kernien et al., 2018). These communities adhere to all different types of surfaces, on which they form complex structures that allow them to grow and protect themselves. Biofilms can grow on almost any surface, both biological and non-biological (Donlan, 2002). Microplastics provide an attractive surface for biofilms to colonize, due to their developed surface roughness from weathering as well as their natural hydrophobicity—two factors that have proven to promote biofilm formation and diversity (Donlan, 2002). Biofilm formation begins as soon as an initial microorganism comes into contact with any surface.

Though the microorganisms comprising biofilms are diverse, there are four common stages to biofilm formation; these include (1) attachment to the surface, (2) adhesion and formation of the microcolony, (3) maturation of the biofilm and finally (4) dispersion of the bacteria, which restarts the formation process (Crouzet et al., 2014). The initial stage of biofilm formation starts when microorganisms are free-floating within the environment of interest and come into contact with an attachable surface. This can be anything, commonly including wood, metal, rocks, glass, and of course plastics. From there, the newly attached microorganisms begin to produce a slimy, glue-like substance that strengthens their attachment to the surface (Vasudevan, 2014). This glue-like material, known as extracellular polymeric substance (EPS), has a strand-like structure that allows the microorganism to bond to the surface as well as to other cells forming the microcolony. This leads to the maturation phase of the biofilm (Vasudevan, 2014), which corresponds to a major period of growth. During this phase, the formation of the EPS continues along with the attachment of more and more microorganisms, which eventually form a three-dimensional, complex structure that is the final form of the biofilm (Donlan, 2001). At any point during biofilm development, cells may detach due to grazing from outside sources or shear stresses from fluid movement in the water column. The detached cells become free-floating microorganisms and restart the biofilm formation process from the beginning (Donlan, 2001).

Though the stages of biofilm formation are relatively similar across a variety of surfaces and microorganisms, the types of bacteria and other organisms comprising each microcolony are unique to the different surfaces to which they adhere. Many studies have shown that the unique properties of microplastics lead to unique microcolonies compared to other natural and unnatural substrates; these colonies also differ amongst different types of plastic (Miao et al., 2019; Oberbeckmann et al., 2018; J. Wang, Lu, et al., 2021; Wu et al., 2019). Biofilms are identified and characterized using a number of different techniques, typically including some form of microscopy or genetic sequencing (Harrison et al., 2018; Tu et al., 2020). Several contradictory studies have

reported on the diversity and richness of microbial communities on microplastics compared to other substrates. For example, Wu et al. (2019) was able to show in freshwater experiments, using a well-known diversity index used in microecological studies (the Shannon-Wiener index), that biofilms on microplastic particles were significantly more diverse (with a higher index value) than those that formed on rocks and leaves. However, a different study using similar identification techniques showed that biofilms on microplastics proved to be less diverse than those that formed on the natural substrates (wood and cobblestone) (Miao et al., 2019). Though the results of these studies are somewhat conflicting, they show that the microbial communities forming on microplastics are indeed unique, attracting a different selection of microorganisms than those found on other substrates.

1.2.3 Factors affecting microplastic biofilm formation

The formation of biofilms on microplastics is influenced by several factors. Environmental factors like nutrient concentration, salinity, temperature, pH levels, and type of flow to which the bacteria and plastics are exposed affect the composition of the communities as well as the overall structure of the biofilm (Pinnell & Turner, 2020; J. Wang, Guo, et al., 2021). Physical properties of microplastics like the type of plastic and the surface roughness have also been shown to affect the formation of biofilms on the surface of plastic particles (Frère et al., 2018; Pinto et al., 2019).

The formation of biofilms is heavily influenced by the environmental conditions to which they are exposed. W. Li et al. (2019) demonstrated that nutrient availability and salinity were the main factors affecting the average growth rate of biofilms, based on their experiments observing colonization characteristics of bacterial communities on microplastics in the Haihe Estuary of Bohai Bay, China. They concluded that the nutrient availability within the estuary had a positive correlation to the average biofilm growth rate, whereas salinity showed a negative correlation to

the average biofilm growth rate. Though excess salinity has been shown to have a negative impact on the growth rate of biofilms, in some cases it has been shown to promote higher diversity in microbial communities (W. Li et al., 2019; Pinnell & Turner, 2020).

pH levels within aquatic environments also play a key role in the survival of microorganisms. It has been observed that there is an optimum pH level for microbial growth, but once levels fall outside the desired range, biofilm growth rate begins to decrease. Auta et al. (2018) showed that microbial growth rate increased in isolate bacteria strains with increasing pH levels until it reached a peak value of optimum growth, but further increase in pH beyond this optimum value led to a decline in the growth of the microbes. Water temperature is also a very important factor in biofilm development. Temperature affects cell growth because it influences enzyme reaction rates (Garrett et al., 2008). Bacterial populations develop more healthily at optimal temperatures, but temperatures outside of the optimal range lower bacterial growth efficiency due to a decrease in the rate of bacterial enzyme reaction (Garrett et al., 2008). Lastly, physical properties of the environment play an important role in the formation of biofilms. In particular, flow conditions are an important factor that influence the formation of biofilms on the surface of microplastics.

The flow conditions within the water column have been shown to impact the physical structure of the biofilm that forms upon a surface. Many studies have compared the architecture of a biofilm formed in stagnant conditions vs. those formed in the presence of increasing flow speeds, and have recorded consistent results (Araújo et al., 2016; Fanesi et al., 2021; Lehtola et al., 2006; Manuel et al., 2007; Park et al., 2011). Manuel et al.(2007) and Lehtola et al.(2006) were both able to show that an increase in water flow rate was positively correlated with an increase in the biofilm growth rate. Lehtola (2006) was able to further show that compositions of the microbial communities on the two tested surfaces – copper and polyethylene pipe – were different in the different flow regimes, indicating a relationship between flow, biofilm formation, and substrate

type. Park et al. (2011) reported in their findings that increased flow rate (which in turn leads to a higher shear stress at the biofilm surface) strongly affects the formation and growth of biofilm. They found that there is an optimal shear stress for the overall growth of biofilms, and that biofilm formation is hindered in both low and high shear stress situations (Park et al., 2011). Araújo et al. (2016) and Fanesi et al. (2021) observed that thicker and more porous biofilms developed in slower flow, and thinner and denser biofilms were formed in faster flow. The results from the above experiments can lead to the conclusion that different flow regimes impact the overall architecture of the biofilm that ultimately forms on a substrate, with a thicker, more porous biofilm in stagnant or low flow regions and a more compact and denser biofilm forming in regions of higher flow speed.

The physical properties of microplastics (size, shape, material, mass density, et al) are also contributing factors to the formation of biofilms upon their surfaces. Several studies have demonstrated that certain types of microorganisms preferentially colonize on different types of plastic (Frère et al., 2018; W. Li et al., 2019; Pinto et al., 2019). Frère et al. (Frère et al., 2018) reported that the polymer family had a major impact on bacterial community composition, with polystyrene (PS) displaying a different bacterial community than polyethylene (PE) and polypropylene (PP). Pinto et al. (2019) also demonstrated similar findings with their experiments, showing that polyvinyl chloride (PVC) had more abundant and diverse microbial communities than those of the other tested polymer types (low density PE, high density PE, PP). They also reported that in the early phases of biofilm development, disparities in the makeup of bacterial communities associated with various plastic surfaces appear to be greater than in later stages of biofilm formation (Pinto et al., 2019). This indicates that the physical properties of the microplastics have a larger impact on the biofilm formation in the beginning stages of biofilm development, when microbes are coming into direct contact with the surface, than in later stages when they are more likely to encounter other microbes already embedded in a developed biofilm.

The surface roughness of microplastics also plays a major role in the formation of biofilms. Once plastic particles enter the environment, they experience different weathering processes, such as (e.g.) shear forces due to grazing (Enfrin et al., 2020) and photodegradation (Yousif & Haddad, 2013) that causes their fragmentation into smaller pieces and increases their overall surface roughness (Andrady, 2017). This increase in overall surface roughness corresponds to an increase in the microbial colonization upon the surfaces. Increased surface roughness increases the overall surface area of plastic particles, which provides more room for microbial attachment as well as a decrease in shear forces experienced by the attached biofilm, which in turn decreases the chance of its detachment (Donlan, 2002).

1.2.4 Effects of biofilms on the transport of microplastic particles

While physical properties of microplastics can promote or discourage biofilm growth, the presence of biofilms on the surface of microplastic particles will also, in turn, affect their physical properties. These include variables like mass density and aggregation potential, which in turn will ultimately affect how the particles behave within the environment. Many studies have shown how the presence of biofilms on the surface of microplastics affects the net density of the plastics (Miao et al., 2021; Semcesen & Wells, 2021; Ye & Andrady, 1991). Kaiser et al. (2017) reported within their findings that the presence of biofilms on the surface of polyethylene microplastics led to a density increase in the plastics, but the plastics did not start sinking below the water surface until they were colonized by mussels. Chen et al. (2019) reported that dense, calcareous organisms such as barnacles and mussels were identified on the surface of larger plastics submerged in the marine environment. The presence of these organisms on the surface of plastics led to a significant impact on their mass. However, in their experiments they found no evidence of calcareous fouling organisms on the surface of microplastics and reported that inorganic minerals trapped during

biofilm growth are likely to be the primary cause of decreased buoyancy in microplastics. These two studies show that the presence of biofilm on the surface of a microplastic does affect its net mass density and in some cases can cause a loss of buoyancy—eventually leading to the sinking of plastics within the water column.

An increase in a microplastic's mass density causes a change in its buoyancy, and could potentially lead to the sinking of some types of plastics that typically float in water (i.e., HDPE, LDPE, PP, etc.) (Chen et al., 2019; Semcesen & Wells, 2021). These changes in density and buoyancy will redistribute microplastics within the water column to a stable location; the addition of biofilm can even cause microplastics to sink all the way to the bottom of water column, where they are often buried in sediment (Leiser et al., 2021; Pohl et al., 2020). This vertical transport can also be more complicated: Ye & Andrady (1991) concluded that floating plastic debris was quickly fouled at the surface of the water, but once the debris was submerged, it most likely sank to the mid-water column, experienced loss of biofilm, and then resurfaced to repeat the cycle without ever actually reaching the sea floor. This indicates that the transport processes of biofilm-covered microplastics is much more complex than the particles simply gaining mass and sinking below the surface of water to end up embedded in bottom sediments, though this is likely what happens over a very long time scale (López et al., 2021).

Sinking due to added mass from biofilms is not the only pathway for the removal of microplastics from surface waters. Biofilm formation leads to the production of extracellular polymeric substance (EPS), which is the sticky, glue-like substance that holds the whole biofilm together and allows for the attachment of additional microorganisms, creating a fully mature, three-dimensional biofilm (Vasudevan, 2014). Several studies have shown that the presence of the EPS matrix on the surface of microplastics increases the aggregation potential of microplastics with other sediments that are present within the water column (Long et al., 2015; Lagarde et al., 2016; Michels et al., 2018). Long et al. (2015) showed that when microbeads were exposed to

phytoplankton aggregates, they became entangled within those structures and changed the overall sinking rate of the “hetero-aggregate”; they conclude that natural aggregates serve as a sink for microplastics within aquatic environments, and affect their transport within the environment.

While significant gaps remain in our knowledge of microplastic transport in relation to biofilm development, it is clear that biofilms strongly affect important physical properties of microplastics. However, more research is needed to understand the effect of biofilms on larger-scale transport processes to better understand the ultimate fate of microplastics within the environment.

1.2.5 Risks posed by biofilmed microplastics

Biofilm-developed microplastics have been shown to have a greater affinity to pollutants than virgin microplastics, perhaps posing a greater risk within aquatic environments (Guan et al., 2020; Richard et al., 2019; Y. Wang et al., 2021). Richard et al. (2019) and Y. Wang et al. (2021) demonstrated that the amount of biofilm on a plastic surface was positively correlated with metal accumulation. Several other studies have shown that biofilmed microplastics are more inclined than virgin plastics to sorb both heavy metals (Guan et al., 2020; Stenger et al., 2021) and harmful pathogens (Pham et al., 2021). Microplastic particles have also been shown to attract polychlorinated biphenyls (PCBs) and polycyclic aromatic hydrocarbons (PAHs) (Caruso, 2019; Ziccardi et al., 2016), two classes of chemical compounds that can have toxic effects on living things. PCBs, PHAs, and microplastics are all hydrophobic substances—since most plastics are also hydrophobic, these compounds are pushed toward one another (Ziccardi et al., 2016). When microplastics—biofilmed or otherwise—are consumed by aquatic organisms, both microplastics and harmful contaminants enter the food chain.

Microplastics are ingested by a variety of creatures, including crustaceans, barnacles, fish, turtles, birds, and whales (J. Wang, Guo, et al., 2021). Some organisms are drawn to directly ingest microplastic particles because the nutrients they typically consume are present within the biofilms on the surface of the plastics (Carson, 2013). Savoca et al. (2017) reported that odors linked with biofouled plastic litter elicited a foraging response in captive anchovy schools, whereas virgin plastics did not induce changes in their behavior. Fabra et al. (2021) reported that the presence of biofilms on microplastics made them more likely to be ingested by filter feeding organisms (oysters) when compared to virgin microbeads with no biofilm development. While these studies and others have explored the tendency of aquatic organisms to ingest microplastics, less is known about how microplastics – once ingested – can impact the health of those organisms. Once the particles have been ingested, they can cause damage both physically (clogging of guts or lacerations from sharp edges) and chemically (transferring harmful contaminants embedded in biofilms or chemically sorbed to the plastic) (Horton & Dixon, 2018). The trophic transfer of biofilm-developed microplastics can lead them to be ingested humans as well, thus indicating that biofilmed microplastics may also pose unknown risks to human health (Froelich et al., 2012; Heithoff & Mahan, 2004).

Many humans regularly consume aquatic organisms, so the potential for incidental consumption of microplastics is very high. Saha et al. (2021) reported the presence of microplastic particles in many of the marine organisms present in the Sal estuary on the central west coast of India – specifically in shellfish, which is commonly consumed in that region. Many studies have also reported the presence of microplastics in drinking water (Johnson et al., 2020; Koelmans et al., 2019a, 2019b; Novotna et al., 2019). Cox et al. (2019) conducted an experiment based on a number of different foods and the amount of microplastics found in them to estimate the annual intake of microplastic particles by humans. They reported that each person may be consuming 39,000 to 52,000 microplastic particles per year. In spite of these alarming figures, there is very

limited information on the short-term and long-term health effects of microplastics on the human digestive system, so this remains a priority research topic (Horton & Dixon, 2018).

1.3 Effects of spatial inhomogeneity of mass density on settling velocity

The effects of biofilm on the settling behavior of microplastics has been a recent area of interest, but it has only been explored in a very general sense—that is, if biofilm is present, it causes a change in the settling velocity of the microplastic (Chen et al., 2019; Miao et al., 2021; Semcesen & Wells, 2021). However, a largely overlooked topic is the non-uniform formation of biofilms on the surface of microplastics, and how the spatial distribution of biofilm may affect the behavior of microplastics. The majority of plastics are buoyant, and typically float until enough biofilm develops upon their surface and induces sinking (Chen et al., 2019). This appears to suggest that the initial biofilms that come into contact with microplastics preferentially develop on the submerged side; this uneven development may have a substantial impact on mass distribution and thus settling velocity. An offset in the center of mass (COM) of a particle introduces different dynamics to a particle's settling behavior—for example, the added mass creates torque that can cause the particle to continuously rotate, or rotate until it reaches a stable position, which in turn affects the settling speed of a particle (Abelev et al., 2007; Chu et al., 2002; Will & Krug, 2021).

Few studies have demonstrated how a nonuniform mass density can alter settling velocity and behavior. Abelev et al. (2007) showed for cylindrical particles that when the center of mass was farthest from the geometric center of the cylinder, it reached a greater terminal velocity. (Angle et al., 2019) reported for uniform and non-uniform density cylinders that both shape and density homogeneity affected the overall settling velocity and the cylinder orientation and trajectory as it settled. The results from these two studies clearly show how the spatial inhomogeneity of mass

density can affect the settling velocity of different particles, but this has not been examined in the context of biofilmed microplastics.

The studies mentioned above demonstrate how variations in the center of mass across different particles affect their settling velocity and overall settling behavior. Since biofilms are likely to form on the surface of microplastics in a non-uniform way, this indicates that spatial inhomogeneity may also affect the settling behavior and transport of microplastics. It is therefore important to expand the study of how biofilms affect the transport of microplastics to include not just bulk effects, but detailed analyses of how the spatial distribution of biofilm can impact a microplastic's settling behavior.

1.4 Motivation for studying the effects of biofilm on the transport of microplastics

Nurdles and the plastic items formed from them can infiltrate the environment through a variety of pathways—for example, runoff from environmental processes or microfibers shed from clothing. Whether primary (introduced as small particles) or secondary (weathered into small particles), these microplastics provide a fresh surface for biofilm formation. The presence of biofilm on the surface of microplastic particles will impact their physical properties, which will influence how they behave in the environment: where they go, how long they stay, and what eventually happens to them. As discussed in Section 1.2.5, biofilmed microplastics have an affinity for surface contaminants compared to non-biofilmed microplastics, perhaps posing a greater risk to aquatic organisms and increasing the risk of harmful contaminants being transferred to the animals and humans that interact with these environments.

We are motivated to fill a major gap in our understanding of how biofilms affect microplastic transport. While several studies have looked at how the overall presence of biofilms can affect transport properties, this is typically treated as a bulk effect—either biofilms were present

on the plastic, or they weren't. There are currently no studies of how the non-uniform spatial distribution of a biofilm affects the transport of microplastics. Because most plastics are positively buoyant, it is likely that biofilms preferentially colonize on the submerged side of plastics. Uneven mass distributions in other types of particles have been shown to affect import transport parameters such as settling velocity; since uneven mass distributions are also likely to occur in microplastics, more research should be done to explore the potential effects of non-uniform biofilm development on the settling behavior of microplastics.

Our study is the first to investigate how an uneven mass distribution of biofilm – that is biofilm concentrated on a single side of a microplastic – on the surface of microplastics affect their rising velocity, tumbling rate, and lateral motion when compared virgin microplastics and microplastics that have biofilm present all over their surfaces. We first introduced a bacterial biofilm to the surface of high-density polyethylene nurdles in which we allowed the biofilm to grow on one side of the nurdles by leaving the nurdles to float undisturbed in a flask with the biofilm. In a second growth period, we introduced the nurdles to the biofilm in the flask, but this time gently rotated the flasks on a daily basis to allow biofilm to colonize on all sides of the plastic. Once the biofilm growth was sufficient enough for both growth regimes, we recorded their rising behavior as the rose to the surface of our constructed rise tank. We then characterized the biofilm on the plastic surface under a microscope then went on to remove the biofilm from the plastic surface and repeated the process of putting the nurdles through the rise tank for the naked nurdles. With the information gathered from our experiments, we take steps to answering important questions about how the spatial distribution of biofilm on the surface of a microplastics affects their settling behavior in the natural environment.

Chapter 2: Methods

2.1 Material selection and density measurement

Many different polymers are used in the production of plastic products; for our experiments, we selected high-density polyethylene (HDPE). We chose this material because it is one of the most abundant buoyant plastics (along with polypropylene) used in the manufacture of plastic goods around the world and has been experimentally shown to allow for the growth of biofilms upon its surface (Amaral-Zettler et al., 2021; Andrady, 2017; Lagarde et al., 2016). A sample of high-density polyethylene resin was provided to us by Bay Polymer LLC (Fremont, CA). The sample consisted of small (~3mm) pieces of plastic (nurdles), roughly in the shape of short cylinders or thick disks (see Figure 1).

Figure 1. Example of high-density polyethylene (HDPE) nurdles used to conduct experiments.

Mass density of the HDPE sample was not provided; however, knowledge of this property would allow us to predict the nurdles' approximate settling velocity and the biofilm thickness required to nontrivially alter the settling/rising velocity of the nurdles. The typical range of values for the density of HDPE can range anywhere from 0.84 – 0.97 g/cm3 (Manjula et al., 2017). We measured the density of our HDPE nurdles at Penn State's Materials Characterization Laboratory (MCL) using a Helium Pycnometer (Micromeritics Accupyc II 1340). This instrument measures the amount of helium that is displaced by the sample within a chamber of known volume, returning a precise volume measurement of the sample within the chamber. The mass of the sample is measured on a precision scale; the quotient of mass and volume is the density. The mass and volume measurements of the sample were performed 10 times on a 3.5 cubic centimeter (cc) volume filled with nurdles and averaged for accuracy. The average of the 10 density measurements was 0.9315 ± 0.0004 g/cm³, which falls within the expected range for the density of HDPE (0.84 – 0.97 g/cm^3 (Manjula et al., 2017)).

2.2 Bacterium selection and biofilm growth procedure

A live culture of filamentous, un-branched Cyanobacteria of the genus *Anabaena* (species unknown) was purchased through Penn State's Avantor Stockroom and supplied by the University of Texas at Austin. This specific genus of bacteria was chosen because it is commonly found in freshwater systems and is known to colonize the surface of plastic particles, particularly on the surface of HDPE (Vimal Kumar et al., 2017). It was also chosen because it is a photoautotroph: it can produce its own food by using light and nutrients that are present in the surrounding water. This simplified the bacterial culturing process for feasibility in an engineering laboratory, and also mimics a potential microplastic colonization scenario in a nutrient-limited system dependent on

phototrophic productivity. The bacterium was inoculated into two 500-mL Erlenmeyer flasks containing Basic Algae Culture Solution, also purchased through Penn State's Avantor Stockroom and provided by Ward's Science. The HDPE nurdles were sterilized in 91% Isopropyl Alcohol for 1 hour before being introduced into the Erlenmeyer flasks with a sterilized pair of cross-lock tweezers to prevent any cross contamination into the bacterial culture. The positively buoyant nurdles floated at the surface of the medium. After the nurdles were introduced, the flasks were placed on a clear Plexiglas stand; a white LED panel introduced light to the bottom of the culture and fluorescent LED tube lights overhead introduce light to the top. Both light sources were controlled by a switch timer that was set to a photoperiod of 12 hours (light) + 12 hours (dark). The cultures were maintained for the entire growth period at room temperature, which was measured to be approximately 70.0 ± 1.5°F.

In the first growth regime (BF1), the nurdles were left undisturbed to grow under the light sources for 9 weeks. Biofilm grew only on the submerged side. The nurdles in the second growth regime (BF2) were grown under the same conditions, but flasks were gently turned (+180 degrees and then -180 degrees, three times, once a day for the full growth period) to introduce all sides of the nurdles to the culture medium and allow growth on all surfaces. BF1 and BF2 were grown sequentially in February – May 2022. Growth of the biofilms on the surface of the plastics was qualitatively monitored for the two growth regimes by removing a small number of nurdles from the flasks every two weeks and examining under a microscope (Axiophot Photomicroscope, Zeiss).

2.3 Experimental setup

A diagram of the experimental facility used to measure the rising nurdles can be seen in Figure 2. It consisted of a square cross-section acrylic water tank (30.5 in. in height, with a width of 5 in.) filled with still (fresh) water, a piece of PVC vinyl tubing (46 in. in length with a half in.

outer diameter) connected to a half inch hose barb and clamped with a stainless-steel hose clamp to prevent leaking. The hose barb was threaded into the center of the bottom of the acrylic tank and connected to the tubing with the hose clamp as shown. The PVC tubing was longer than the overall height of the tank to use the principle of hydrostatic equilibrium—as long as the open end of the tubing remained at a height at or above the water surface within the acrylic tank, the tank would not drain – the heights of water in the tank and in the tube would remain the same. This simple configuration allowed us to easily introduce the HDPE nurdles to the bottom of the tank without disturbing the water within the tank. We placed the nurdles in the open end of the PVC tubing with a pair of tweezers when it was still in its elevated position, then blocked the tubing with a thumb or hand to prevent any water or the nurdle from escaping the tube, and then finally rotated the tube 180° and lowered the open end several feet below the bottom of the acrylic tank. The nurdles' buoyancy would then slowly force them through the tubing and hose barb to enter and then rise to the top of the tank.

Two high speed cameras (Chronos 1.4, Krontech) captured the rising microplastics through overlapping 4 × 4 in. fields of view centered on orthogonal walls of the acrylic tank and positioned 26 in. above the tank floor. The cameras, filming at 500 frames per second, were synchronized in time and triggered to record simultaneously using an external push-button BNC switch. Two white LED light panels provided diffuse backlit illumination for the high-speed cameras. The entire facility was mounted on top of a large optical table.

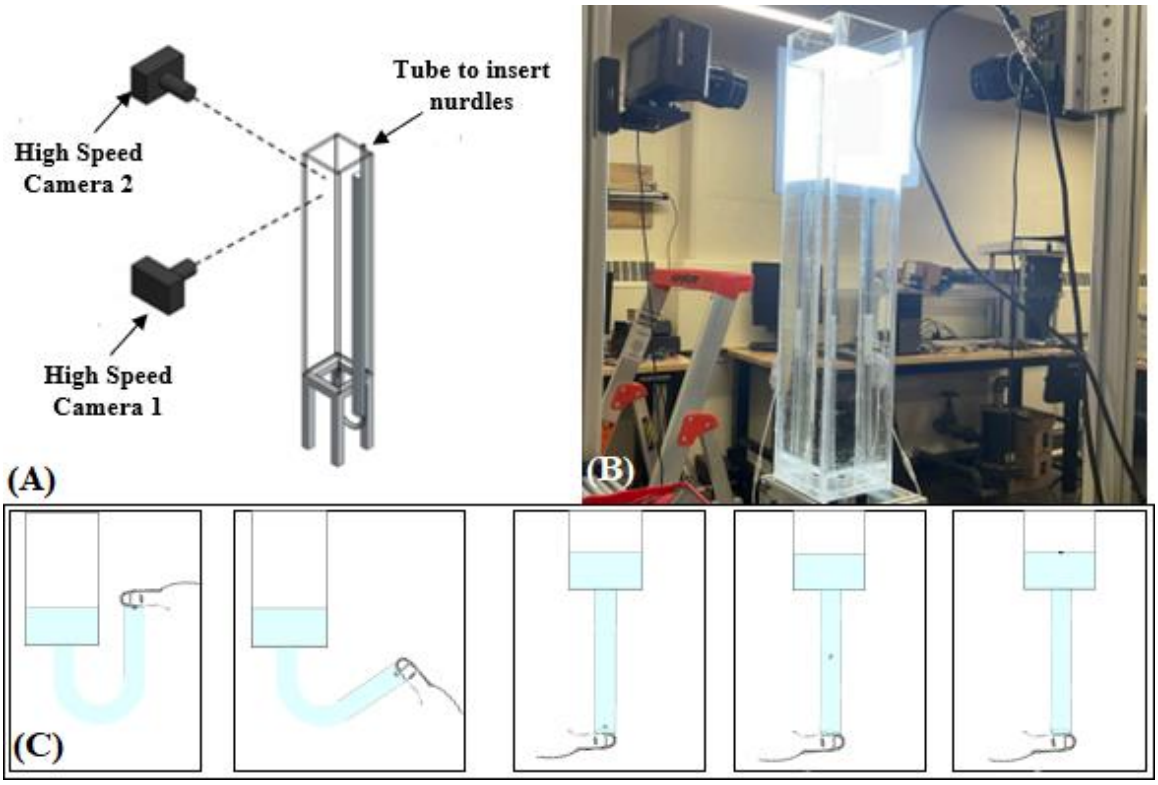

Figure 2. (A) Experimental setup showing positioning of tank, nurdle entrance port and tubing, and orthogonal high speed cameras (LED panels not shown). (B) Photograph of facility. C) Schematic of nurdle introduction via vinyl tubing (tank height not to scale).

A total of 100 nurdles were released into the facility described above: 50 from each growth regime (non-uniform, one-sided growth (BF1) and uniform, two-sided growth (BF2)). First, the biofilmed HDPE nurdles were released into the tank and videos of their rising were captured simultaneously from the two cameras. Each individual nurdle was put through the tank until a total of five successful trials were recorded, where a successful trial was defined as one in which the rising nurdle passed through the field of view of both cameras. Table 1 shows example data for the average standard deviation of rise velocity across five trials of a single nurdle compared to the standard deviation of the mean rise velocity across all 50 nurdles. For each case, the mean standard deviation across the five trials of a single nurdle in all treatment groups is at least 3 times smaller than the standard deviation of the mean rise velocity across all 50 nurdles. These data show that there was not a large amount of variability from test-to-test with the same nurdle compared to the

variability across nurdles, and that the average of the five trials for a single nurdle is most likely representative of the individual nurdle's overall behavior. After rising behavior was recorded, the biofilmed nurdle was placed in a water-filled petri dish and stored in a refrigerator to pause biofilm growth until the nurdles could be characterized under the microscope (as described in section 2.4). After the nurdle's biofilm coverage was characterized under the microscope, it was carefully cleaned by being soaked in bleach for one minute and wiped down with ethanol wipes to remove all presence of the biofilm. After cleaning, the "naked" nurdle was released into the tank once more until five successful trials were recorded of the rise behavior. This process enables a direct comparison between the same nurdle with and without the presence of biofilm to more directly observe the effect of biofilming on the rising behavior of the microplastics. Measurements were completed sequentially: we first measured biofilmed rise velocity for all 50 BF1 nurdles, then biofilm coverage for all 50 BF1 nurdles, then rise velocity for all 50 BF1 nurdles after the biofilm was removed (which we label N1). The process was repeated for the BF2 nurdles, which were labeled N2 after biofilm was removed.

Table 1. Example data to show the variability across 5 trials for one nurdle as it rose through the rise tank compared to the overall standard deviation of the rise velocity across all 50 nurdles. Inter-nurdle variability is generally at least three times larger than intra-nurdle variability.

Treatment Group	Average standard deviation of rise velocity within one nurdle across 5 trials	Standard deviation of mean rise velocity across all 50 nurdles
BF1 Camera #1	0.22	0.69
BF1 Camera #2	0.21	0.70
N1 Camera #1	0.26	0.77
N1 Camera #2	0.20	0.77
BF2 Camera #1	0.14	0.79
BF2 Camera #2	0.15	0.78
N2 Camera #1	0.20	0.66
N2 Camera #2	0.20	0.66

2.4 Biofilm characterization

To verify the presence of biofilm on the surface of the nurdles, we examined the biofilmed nurdles under a light microscope (Axiophot Photomicroscope, Zeiss). We took images using a microscope camera (MU1000, AmScope) for each individual nurdle in each growth regime (BF1 or BF2). *Anabaena* cells exhibit autofluorescence: when they are excited with a specific wavelength of light, they will emit a different wavelength of light indicating their presence on a surface without the need for fluorescent staining (which could damage the sample). The biofilmed microplastics were placed under the microscope on a slide and illuminated by green light from a mercury arc lamp, inducing red autofluorescence. We then reoriented the nurdle until the maximum possible biofilm coverage was qualitatively judged to be visible on its surface. We took a photograph of the green-illuminated sample, then illuminated the same nurdle (in the same position) with white light and took an additional photo for later identification of the nurdle's edges.

All of the images of the non-uniformly biofilmed nurdles (BF1) were taken with a 5x objective lens and an exposure time of 300 ms. All of the images of the uniformly biofilmed nurdles (BF2) were taken with a 10x objective lens and exposure time of 500 ms. The difference in the exposure time between the two treatment groups was selected due to the difference in visibility of biofilm on the surface of the nurdles across the two treatment groups. It is possible that BF1 developed a thicker layer of biofilm than BF2, as indicated by the difference in exposure time needed to capture overall biofilm coverage in the microscope images between the two treatment groups. However, this is not consistent with our qualitative observations. We discuss this possibility further in section 3.5.

Postprocessing of the microscope images was done in ImageJ (Rasband, W.S., ImageJ, U. S. National Institutes of Health). First, the green illuminated image was converted to a grayscale image. Next, we set a lower limit of 9 pixel intensity units for the threshold value so that only the

biofilm emission was highlighted within the image. This threshold was selected to match the qualitatively-determined boundaries of the observed biofilm. From there, we used ImageJ to measure the size of the highlighted area included in the highlighted area. The same process was repeated for the white light images, but the threshold value was set to an upper limit of 10 pixel intensity units to identify the edges of the entire nurdle within the image and only the area of the nurdle was recorded (we note that the overlap in the two intensity thresholds is coincidental, as they were applied to two different images under different lighting as shown in Figure 3). Again, this threshold was qualitatively determined to match the observed boundaries of the nurdle. Figure 3 shows some example images our biofilm characterization process. Finally, we divided the area of the biofilm by the area of the overall nurdle to serve as a measurement of biofilm coverage. We measured the biofilm coverage for each individual nurdle that had a high-quality corresponding image of the biofilm (N=34 for BF1 and N=40 for BF2). A minority of nurdles in each sample was difficult to image or sustained damage to their biofilm between testing of their rise velocity and microscopic imaging.

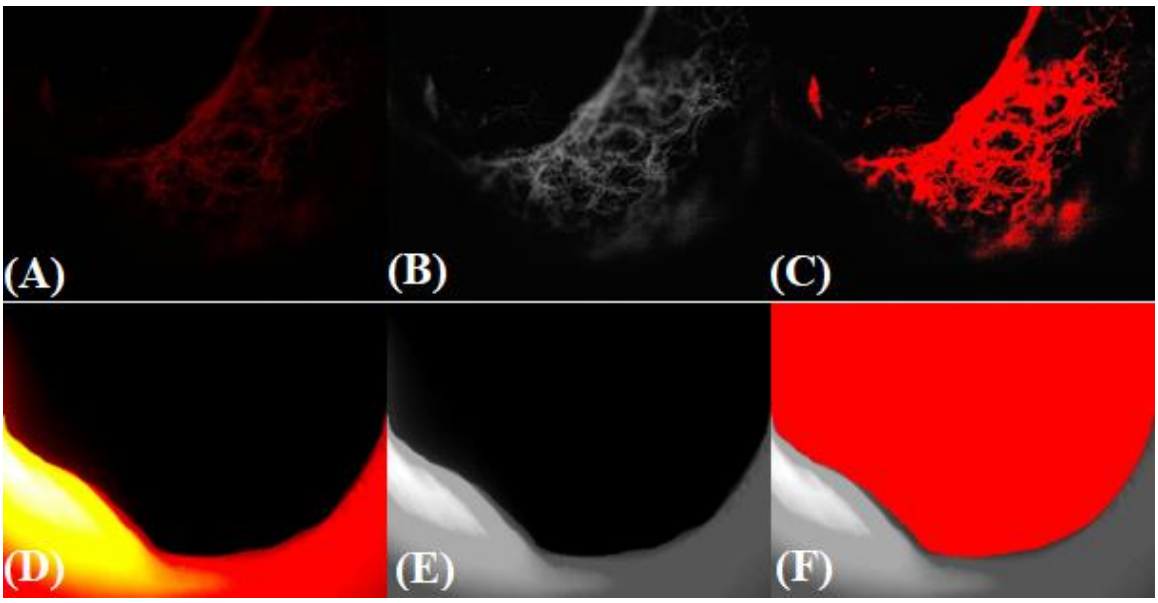

Figure 3. Example images from biofilm characterization process. Panels (A) through (C) are the characterization of the green-light illuminated images: (A) raw image with red emission, (B) image converted to grayscale, and (C) image with thresholding, with the biofilm highlighted in red. Panels (D) through (F) demonstrated the same process, but for a white-lit image of the nurdle (in the same exact position as in the green-light image) to identify the overall nurdle area highlighted in red in panel (F). Nurdles were qualitatively positioned so that the maximum biofilm coverage would be visible.

2.5 Nurdle rise kinematics

To determine the rising characteristics of the nurdles, videos from the two high speed cameras (Figure 4) were used to track the nurdle's position in each camera's two-dimensional view. Each camera view was calibrated to real space with a reference distance on a calibration plate deployed within the field of view (LaVision GmbH). Three-dimensional calibration information was collected, but not used in analysis. Each video frame was binarized using the edge() command in MATLAB, which looks for maximum values of the image intensity gradient as calculated using the derivative of a Gaussian filter. The command returns a binary image, with ones where the function finds edges of an object and zeros everywhere else. The identified objects were then filled, showing a white region (the nurdle) on a black background. Due to uneven lighting or air bubbles present within the tank, the binarization often yielded several white regions within the image that

were not consistent with actual position of the nurdle; additional processing steps eliminated this noise via thresholding for expected values of area and circularity consistent with validated images of nurdles. A final processing step eliminated noise regions that fell within the measured parameters of the nurdles: if the filtered video frame showed zero or greater than one nurdle, it was not considered in the timeseries of calculated parameters. The end result was a sequence of binary images in which the nurdle appeared as a single white area within the image on a black background. Figure 4 shows an example raw video frame, binarized/filled video frame, and a frame in which only the nurdle itself is highlighted.

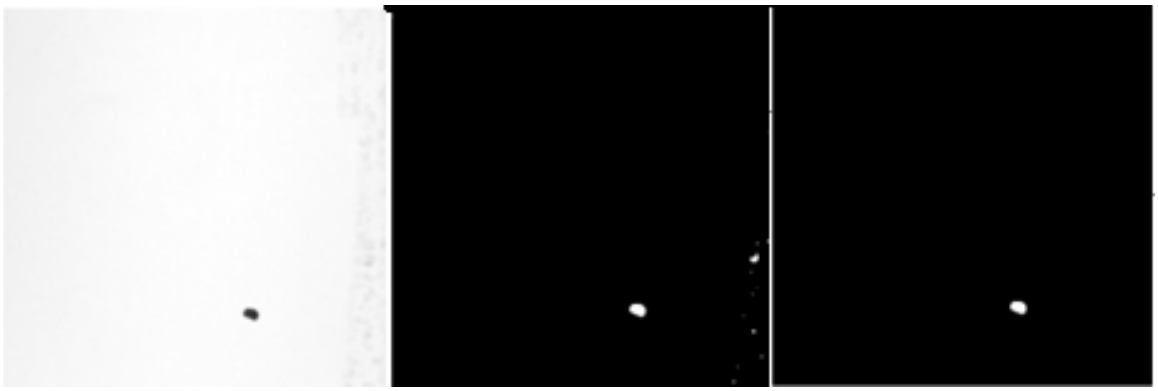

Figure 4. Sample frames from high-speed videos of the HDPE nurdles. MATLAB image processing tools are used isolate the nurdle numerically from the background creating black and white binary images at right with only the nurdle in frame.

Once the binarization of the image was completed, we used MATLAB's built-in functions to measure the x- and y-position of the nurdle centroid, the projected area of the nurdle, and the perimeter of the nurdle for each frame for each camera, yielding a timeseries of these properties as the nurdle passed through the cameras' fields of view. The rise velocity of the nurdle was determined using central differencing of the tracked y-position of the nurdle and the known time difference Δt=2 ms between each frame:

$$\left(\frac{dy}{dt}\right)_i \approx \frac{y_{i+1} - y_{i-1}}{2\Delta t}$$

where y_{i+1} is the vertical position of the nurdle at the $i + 1^{\text{th}}$ frame, y_{i-1} is the vertical position of the nurdle at the $i - 1^{\text{th}}$ frame, and $\left(\frac{dy}{dt}\right)_i$ is the approximate rise velocity at the i^{th} frame. The rise velocity, projected area, projected perimeter, and x-position all varied with time as the nurdle rose through the tank. In the next section, we analyze how these properties vary between the two growth regimes and between biofilmed vs. naked nurdles.

Chapter 3: Results

3.1 Nurdle rising velocity

Figure 5 shows an example of the timeseries data extracted from videos (Figure 5A) of a rising nurdle; this specific case shows a non-uniformly biofilmed nurdle (BF1). These data include the nurdle's vertical (y-) position, which is used to calculate the nurdle's rise velocity (Figure 5B); the nurdle's horizontal (x-) position over time (Figure 5D); and the nurdle's projected cross-sectional area over time (Figure 5C). The variation of area over time served as a proxy to quantify the tumbling behavior of the nurdles as they rose (projected perimeter over time was also measured, but showed similar trends to area and was not analyzed). These data, collected from two simultaneously recording orthogonal cameras, allow us to directly compare the behavior of the five experimental treatments – naked nurdles (N0, N1, N2), non-uniformly biofilmed nurdles (BF1), and uniformly biofilmed nurdles (BF2). We are confident that the nurdles reached their terminal rising velocity based on the typical (unfiltered) velocity timeseries plot shown in Figure 5B, calculated via central differencing of the y-position. The vertical velocities of the nurdles over time demonstrated small fluctuations about a constant average, indicating that they were rising without acceleration. We designed our rise tank based on similar studies which explored the settling and rising behavior of microplastics (Semcesen & Wells, 2021; Waldschlä & Schü, 2019).

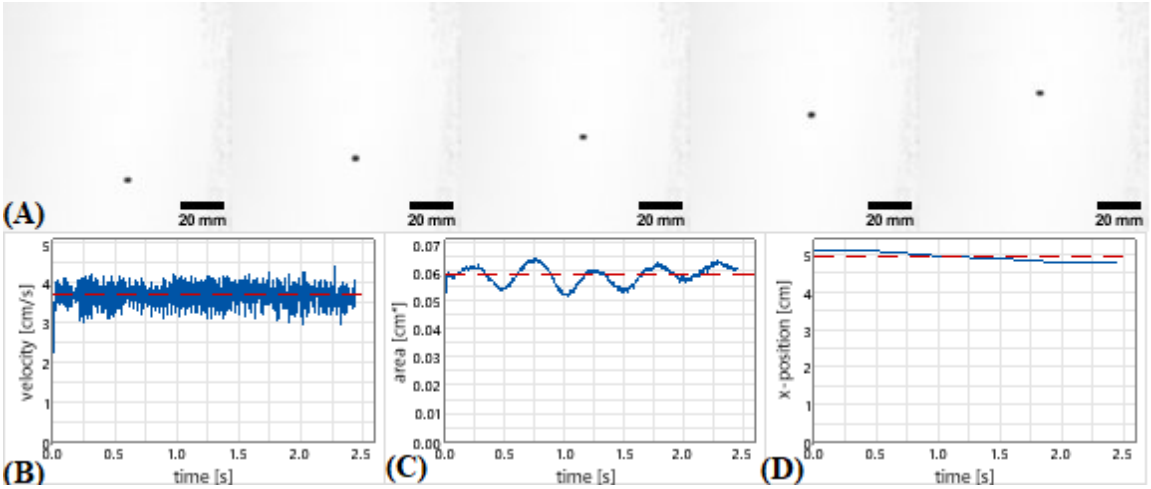

Figure 5. Example of timeseries data of a rising non-uniformly biofilmed (BF1) nurdle, collected from a single camera. (A) Sequence of video frames of a nurdle rising through the water tank. Images are separated by a time interval of $\Delta t = 2\ ms$ (B) Timeseries of rise velocity, calculated via central differencing of the tracked vertical (y) position of the nurdle. Red line represents the time-averaged rise velocity of 3.68 cm/s for this case. (C) Timeseries of projected area of rising nurdle, measured as a proxy for nurdle tumbling. The measured range of this quantity was compared between two orthogonal camera views to determine maximum tumbling. Red line represents the average area of the nurdle at 0.059 cm^2 for this case. (D) Timeseries of tracked lateral (x) position of rising nurdle, with red line representing the time-averaged x-position of the nurdle at 4.95 cm for this case. The standard deviation of this quantity was compared between two orthogonal camera views to determine maximum lateral position variation.

First, we compared the rising velocities of the different experimental treatments of the nurdles (Figure 6). For each trial, rising velocity was time-averaged over the duration of the recorded video, and then averaged between the two camera views. Each nurdle was recorded 5 times, and the rise velocity from each trial was then averaged to calculate the data shown in Figure 6. Figure 6A shows a histogram of the settling velocities of the naked nurdle experimental groups (N0, N1, and N2). The groups N1 and N2 are nurdles that had biofilm grown on them during the nine week growth period described in Section 2.2, and comprise the same nurdles as BF1 and BF2 respectively. After BF1 and BF2 were measured, the biofilm was removed as described in Section 2.3 and the groups were relabeled N1 and N2. Group N0 was a control group of nurdles that never had biofilm grown upon them. The resulting analysis shows that the mean rise velocity is not significantly different between groups of nurdles that do not have biofilm present on the plastic surface, whether they never had biofilm on their surface or if the biofilm was removed as described

in Section 2.3. The histogram in 6A shows significant overlap between the rising velocities for the N0, N1, and N2 cases. We compared the mean rise velocities of the naked nurdles using an analysis of variance test (ANOVA); the means were not significantly different between the three treatments ($p = 0.472$).

Figure 6B shows a histogram of the rise velocities of the nurdles in the naked (N1) vs. non-uniformly biofilmed (BF1) treatments. The nurdles in the BF1 and N1 treatments are phyically the same nurdles; experiments were first conducted on biofilmed nurdles (BF1), then the biofilm was then cleaned from the surface of the nurdle and experiments were conducted on the resulting naked nurdles (N1). The average rise velocity for BF1 is 4.85 cm/s and the average rise velocity for N1 is 5.51 cm/s.

Figure 6C shows a histogram of the rise velocities of nurdles in naked (N2) vs. uniformly biofilmed (BF2) treatments. The nurdles in the BF2 and N2 are also physically the same nurdles, and went throught the same treatment process described for BF1 and N1. The distributions of the measured rise velocities are similar between the two treatment groups. The average rise velocity for BF2 is 5.35 cm/s and the average rise velocity for N2 is 5.64 cm/s. For direct cross-comparison, the rise velocities of the non-uniformly biofilmed (BF1) and uniformly biofilmed (BF2) nurdles are also shown (Figure 6D). The histograms of these two treatment groups do not completely overlap.

We performed another ANOVA test on the four treatment groups shown in Figures 6B – 6D (BF1, N1, BF2, and BF2). The results show that at least some treatments are significantly different from one another ($p < 0.001$). We extended the analysis with a Tukey pairwise comparison test (Table 2), which showed that the mean rise velocity of the non-uniformly biofilmed nurdles (BF1) is significantly from the other three groups (N1, BF2, and N2). However, the difference between the mean rise velocities of the uniformly biofilmed (BF2) nurdles and the naked

nurdles (N1 and N2) is not significant at the 95% confidence level. As an additional test, we performed a two-sample t-test on BF2 vs N2, which showed that the mean rise velocity was different between the two groups at a 90% confidence level ($p = 0.054$). Differences between other pairs of groups, compared via a two-sample T-test, are shown in Table 3.

From these data, we conclude that biofilm distribution affects the rising velocity of the nurdles. Non-uniformly biofilmed nurdles (BF1) showed significantly reduced rising velocities compared to non-biofilmed nurdles (N1). Uniformly biofilmed nurdles (BF2) showed a reduction in rise velocity compared to non-biofilmed nurdles (N2), significant at the 90% confidence level; however, the reduction was not as strong as that of BF1 *vs*. BF2. The one-sided biofilmed nurdles rose, on average, at 88% of their unbiofilmed rising velocity, whereas the uniformly biofilmed nurdles rose, on average, at 95% of their unbiofilmed rising velocity.This implies that two ostensibly equally biofilmed nurdles will rise at different rates if that biofilm is concentrated on one side *vs*. uniformly distributed. This raises the following question: by what mechanism is the rise velocity reduced? We explore possible answers to this question in the following sections.

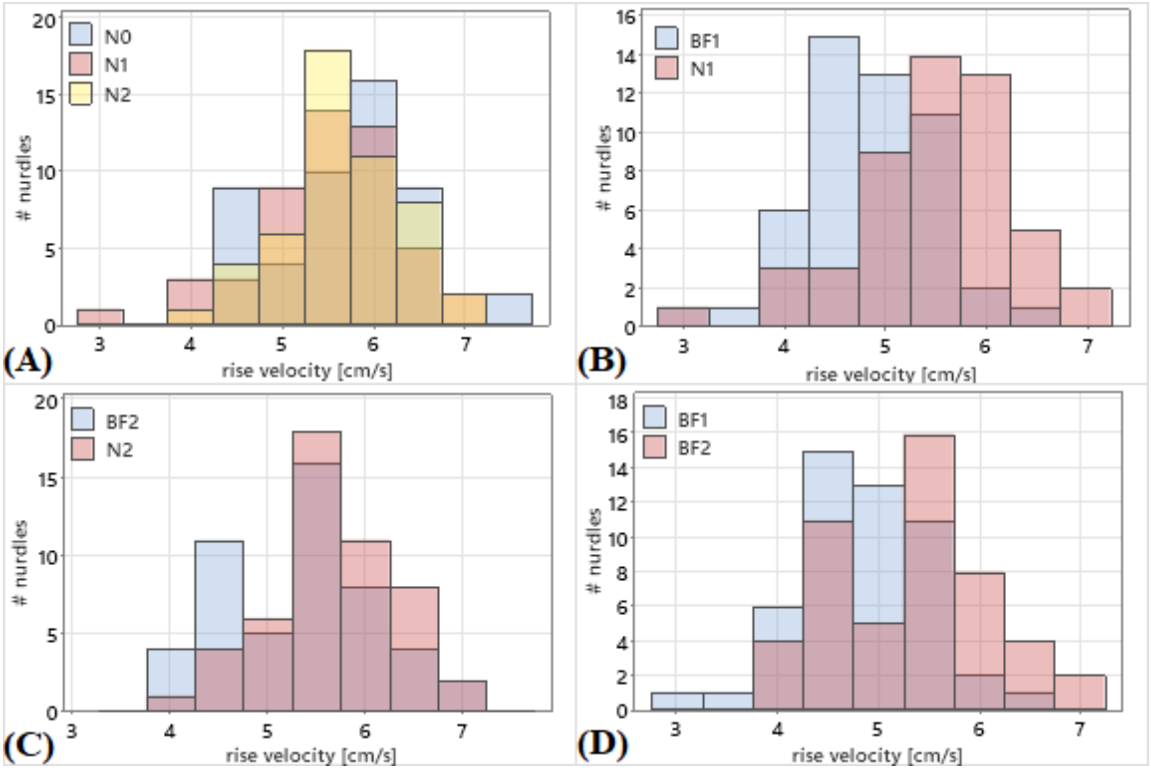

Figure 6. Histograms of nurdle rise velocities, where rise velocity was time-averaged, averaged between two camera views, and averaged between 5 trials per nurdle, with 1 trial per nurdle for N0 (N = 50 nurdles for all groups). (A) Rise velocities of un-biofilmed nurdles (N0, N1, N2); difference between the mean rise velocities were not significantly different between the three groups. (B) Rise velocities of nurdles in naked (N1) vs. non-uniformly biofilmed (BF1) treatments; difference between the mean rise velocities was significantly different between the two groups. (C) Rise velocities of nurdles in naked (N2) vs. uniformly biofilmed (BF2) treatments; difference between the mean rise velocities was not significantly different between the two treatments. (D) Rise velocities of non-uniformly biofilmed (BF1) and uniformly biofilmed (BF2) nurdles; difference between the mean rise velocities was significantly different between the two treatments.

Table 2. Grouping information using the Tukey method with 95% confidence for the rise velocities of naked (N1 and N2) nurdles, non-uniformly biofilmed (BF1) nurdles, and uniformly biofilmed (BF2) nurdles. Means that do not share a letter are significantly different.

Treatment	N	Mean rise velocity (cm/s)	Grouping	
N2	50	5.64	A	
N1	50	5.51	A	
BF2	50	5.35	A	
BF1	50	4.85		B

Table 3. Two sample t-test comparing the mean rise velocities of the non-uniformly biofilmed (BF1), uniformly biofilmed (BF1), and naked (N1 and N2) nurdle treatment groups at 95% confidence level. Includes p-value for each comparison.

Difference between treatments	**Difference of means (cm/s)**	**p-value**
N1 - BF1	0.66	$p << 0.001$
BF2 - BF1	0.50	0.001
N2 - N1	0.13	0.372
N2 – BF2	0.29	0.054

3.2 Nurdle tumbling

We hypothesized that the unequal reduction of the rise velocity of nurdles with different biofilm distributions was due to differences in the tumbling of the nurdles as they rose to the surface of the tank. A nurdle with a higher tumbling rate would experience a higher viscous torque (rotational drag), slowing the overall rise rate. As a proxy for the tumbling rate, we measured the change in projected cross-sectional area of the nurdles as they rose. We calculated the range of measured area (maximum minus minimum observed during the recorded period) to qualitatively determine the overall variability in the tumbling of the nurdles; we took the maximum value between the two simultaneous camera views. For simplicity, we will refer to this variable simply as "tumbling". We first performed this analysis on all the naked nurdle treatment groups (N0, N1, and N2). Figure 7A shows a histogram of tumbling for all the naked cases; the distributions overlap, but the N0 case showed a slightly longer tail toward the right.

We conducted an ANOVA test to measure the variability between the N0, N1, and N2 groups. It revealed that there is a significant difference in mean tumbling between the three naked nurdle groups ($p < 0.01$). The pairwise Tukey comparison (Table 4) revealed that there was not a significant difference in tumbling between N0 and N2 or between N1 and N2, but there was a significant difference in tumbling between N1 and N0. We hypothesize that the difference between

the tumbling of N0 and N1 may be due to less robust measurements of N0, as the data for N0 came from just one video per nurdle, whereas the data for N1 and N2 came from five videos per nurdle. Differences each pair of groups, compared via a two-sample T-test, are shown in Table 5.

Table 4. Grouping information using the Tukey method with 95% confidence for the tumbling of naked nurdle (N0, N1, and N2) treatment groups. Means that do not share a letter are significantly different.

Treatment	**N**	**Mean tumbling (cm^2)**	**Grouping**	
N0	50	0.014	A	
N2	50	0.012	A	B
N1	50	0.012		B

Table 5. Two sample t-test comparing the mean tumbling rate of naked nurdle (N0, N1, and N2) treatment groups at 95% confidence level. Includes p-value for each individual comparison.

Difference between treatments	**Difference of means (cm^2)**	**p-value**
N1 - N0	-0.002	0.005
N2 - N0	-0.002	0.043
N2 - N1	0.000	0.225

Figures 7B through 7D compare tumbling of naked nurdles (N1 and N2), non-uniformly biofilmed nurdles (BF1), and uniformly biofilmed nurdles (BF2). Figure 7B shows a histogram of the non-uniformly biofilmed (BF1) nurdle and naked (N1) nurdle groups. The histogram in Figure 7C shows the overlap of the uniformly biofilmed (BF2) nurdles and the naked (N2) nurdles. Figure 7D compares tumbling of the two biofilmed nurdle treatments (BF1 and BF2), showing similar results to those seen in Figures 7A-C. These results seem to imply low variability of tumbling between the naked (N1 and N2) and the biofilmed nurdles (BF1 and BF2).

We performed an ANOVA test to compare the mean tumbling between the naked (N1 and N2) nurdles, the non-uniformly biofilmed (BF1), and uniformly biofilmed (BF2) nurdles. Tumbling is not significantly different between the four groups ($p = 0.251$). From these results, we conclude that neither the presence of biofilm nor the spatial distribution of biofilm across the nurdle has any

effect on the tumbling of the nurdle, as proxied by the variability of projected area. It is therefore unlikely that the tumbling rate of the nurdle accounts for the change in rise velocity between the different treatment groups.

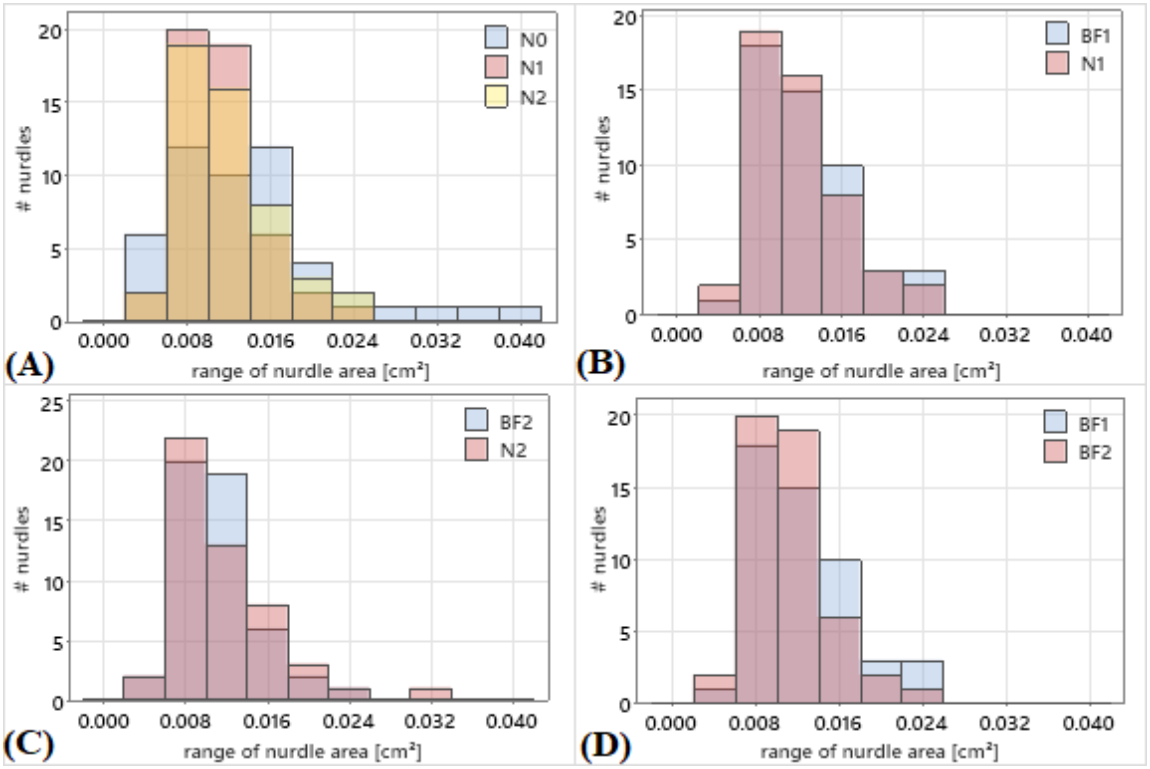

Figure 7. Histograms of nurdle tumbling motion (range of area timeseries), taking maximum value between two cameras (N = 50). (A) Tumbling of naked nurdles; mean tumbling was significantly different between N0 and N1, but not other pairs. (B) Tumbling of nurdles in naked (N1) vs. non-uniformly biofilmed (BF1) treatments; tumbling was not significantly different between the two treatments. (C) Tumbling of nurdles in naked (N2) vs. uniformly biofilmed (BF2) treatments; mean tumbling was not significantly different between the two treatments. (D) Tumbling of nurdles in non-uniformly biofilmed (BF1) vs. uniformly biofilmed (BF2) treatments; mean tumbling was not significantly different between the two cases.

3.3 Lateral motion of rising nurdles

As another potential mechanism for the unequal reduction in rise velocity between BF1 and BF2, we investigated the lateral motion of nurdles within the different treatment groups. We tracked the horizontal (x-) position of the nurdles as they rose and calculated the standard deviation of the x-position over the duration of the recording. We compared the x-standard deviation to see

the variability between different nurdle treatment groups; we will refer to this variable as "lateral motion". We first compared the lateral motion of the naked nurdle treatment groups (N0, N1, and N2) to show that there were no significant differences in lateral motion between previously-biofilmed (N1, N2) and never-biofilmed (N0) nurdles. Figure 8A is a histogram of the lateral motion of the N0, N1, and N2 treatment groups. The large overlap between the lateral motion for the three naked nurdle cases implies that there is not much variability between the N0, N1, and N2 treatment groups. We performed an ANOVA test on the mean lateral motion of the three nurdle groups (N0, N1, and N2) and found that they were not significantly different ($p = 0.177$).

Figure 8B is a histogram of the non-uniformly biofilmed (BF1) nurdles and naked (N1) nurdles, and clearly shows the difference in lateral motion between the two groups. To compare the naked nurdles and the biofilmed nurdles, we performed an ANOVA test on the mean lateral motion of BF1, N1, BF2, and N2, which showed that at least one group is significantly different from others ($p < 0.01$). A Tukey pairwise comparison (Table 6) further revealed that there is a significant difference between the mean lateral motion of BF1 *vs.* N1. Figure 8C compares uniformly biofilmed (BF2) nurdles and the corresponding naked (N2) nurdles, revealing that the two groups have very similar distributions. The pairwise comparison further revealed that there is no significant difference between the mean lateral motion of BF2 and N2. Figure 8D shows the lateral motion of the two differently biofilmed groups BF1 and BF2. There is a significant difference in lateral motion between the non-uniformly biofilmed nurdles and the uniformly biofilmed nurdles (Tables 6 and 7). We performed a two-sample t-test on BF2 vs N2 to see if the difference between their mean lateral motion was significant at a lower confidence level, as we did for the rise velocity. However, the test revealed that the mean lateral motion was not significantly different between the two groups ($p = 0.367$). Differences between other pairs of groups, compared via a two-sample T-test, are shown in Table 7.

From these results, we conclude that biofilm spatial distribution—but not necessarily biofilm presence—affects the lateral motion of nurdles. When the biofilm is concentrated on a single side of a nurdle, there is more side-to-side motion. This is likely one mechanism that lowers the overall rise velocity of BF1 compared to BF2, as increased lateral motion would increase the frictional drag on the nurdle relative to a vertical trajectory.

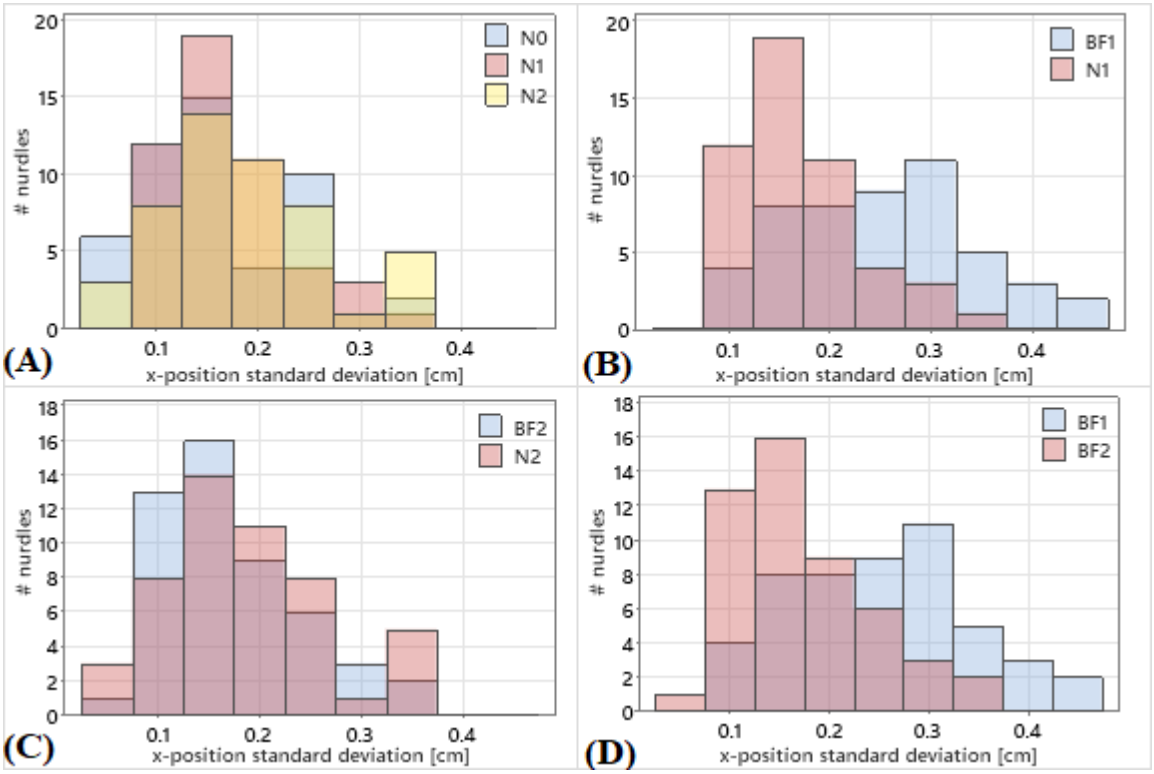

Figure 8. Histograms of nurdle lateral motion (represented by x-position standard deviation), taking maximum value between two orthogonal camera views (N = 50). (A) Lateral motion of un-biofilmed nurdles; difference between the mean lateral motion was not significantly different between the three groups. (B) Lateral motion of nurdles in naked (N1) vs. non-uniformly biofilmed (BF1) treatments; difference between the mean lateral motion was significantly different between the two groups. (C) Lateral motion of nurdles in naked (N2) vs. uniformly biofilmed (BF2) treatments; difference between the mean lateral motion was not significantly different between the two treatments. (D) Lateral motion of non-uniformly biofilmed (BF1) and uniformly biofilmed (BF2) nurdles; difference between the mean lateral motion was significantly different between the two treatments.

Table 6. Grouping information using the Tukey method and 95% confidence for the mean horizontal (x-) position standard deviation of the non-uniformly biofilmed (BF1), uniformly biofilmed (BF1), and naked (N1 and N2) nurdle treatment groups. Means that do not share a letter are significantly different.

Treatment	N	Mean lateral motion (cm)	Grouping	
BF1	50	0.25	A	
N2	50	0.19		B
BF2	50	0.17		B
N1	50	0.17		B

Table 7. Two sample t-test comparing the mean lateral motion of the non-uniformly biofilmed (BF1), uniformly biofilmed (BF1), and naked (N1 and N2) nurdle treatment groups at 95% confidence level. Includes p-value for each individual comparison.

Difference between treatments	Difference of means (cm)	p-value
N1 - BF1	-0.08	$p << 0.001$
BF2 - BF1	-0.08	$p << 0.001$
N2 - N1	0.02	0.204
N2 - BF2	0.02	0.367

3.4 Individual nurdle comparison (rise ratio)

In addition to comparing the overall distribution of the rising velocity between naked *vs.* biofilmed nurdles, we also compared each individual nurdle by defining a dimensionless "rise ratio" RR, where RR is defined as the biofilmed nurdle's rising velocity divided by measured rising velocity of the same nurdle after the biofilm had been removed. Figure 9 shows a histogram of RR for BF1 *vs.* BF2 nurdles, revealing a large difference between the two treatment groups. We performed a two-sample t-test to show that the mean RR is significantly different between BF1 and BF2 ($p \ll 0.01$). We conclude that the ratio of the biofilmed rise velocity to the "naked" rise velocity is also significantly different between the two differently (uniformly and non-uniformly) biofilmed nurdles. The mean rise ratio for BF1 is 0.88, indicating that the rising velocity is reduced by 12% relative to the un-biofilmed case. The mean rise ratio for BF2 is 0.95, indicating that the

rising velocity is reduced on average by 5%, though this difference is at the threshold of significance ($p = 0.054$).

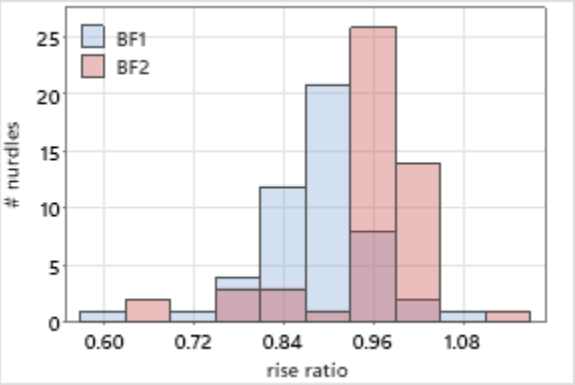

Figure 9. Histogram of nurdle rise ratio for non-uniformly biofilmed (BF1) and uniformly biofilmed (BF2) nurdles, where rise ratio is defined as biofilmed rise velocity divided by un-biofilmed rise velocity and calculated independently for each specific nurdle (N = 50). The mean rise ratio was significantly different between the two treatments.

3.5 Mathematical model of added mass due to biofilm

Both BF1 and BF2 experienced the same growth time of 9 weeks and were grown in identical conditions save the gentle turning that introduced biofilm to both sides of BF2. However, our experimental method did not allow us to directly measure the mass that the biofilm added to each nurdle. A simple mathematical model can illustrate the needed thickness of biofilm to account for the reduced rising velocities we observed. We measured the nurdle density to be $\rho_n = 0.9315 g/cc$. The wet biofilm density is assumed to be $\rho_{bf} = 1.020 g/cc$ (Wäsche & Hempel, 2002). We approximate the nurdle to be a sphere, and assume that it travels at an intermediate Reynolds number ($Re < 2 \cdot 10^5$) with the following drag coefficient (Clift & Gauvin, 1970):

$$C_D = \frac{24}{Re}(1 + 0.15Re^{0.687}) + \frac{0.42}{1 + \frac{42{,}500}{Re^{1.16}}}$$

where $Re \equiv \frac{d_n \rho_f v_n}{\mu_f}$ is the nurdle Reynolds number (d_n is the nurdle diameter, $\rho_f = 1.00 g/cc$ is the density of water, v_n is the terminal rising velocity of the nurdle, and $\mu_f = 1.005 cP$ is the dynamic viscosity of water). The forces on the nurdle include drag, weight, and buoyancy, such that

$$(\rho_f - \rho_n) g \frac{\pi d_n^3}{6} - C_D \rho_f \frac{\pi d_n^2}{8} v_n^2 = 0$$

If the terminal rise velocity v_n is known, we can solve iteratively for d_n. For N1, $v_{n,N1} = 5.51 cm/s$, yielding $d_{n,N1} = 2.98 mm$.

However, if a biofilm of thickness t develops on the surface of the nurdle, the overall diameter increases (increasing drag and buoyancy) and the overall mass increases (increasing weight). For simplicity, we model the biofilm as a uniform thin spherical shell. The new nurdle has diameter $d_{bf} = d_n + 2t$, and a new mass due to the spherical shell of biofilm. The new force balance is

$$\rho_f g \left(\frac{\pi (d_n + 2t)^3}{6} \right) - \left(\rho_n g \frac{\pi d_n^3}{6} + \rho_{bf} g \left(\frac{\pi (d_n + 2t)^3}{6} - \frac{\pi d_n^3}{6} \right) \right) - C_D \rho_f \frac{\pi (d_n + 2t)^2}{8} v_{bf}^2 = 0$$

where the first term is buoyancy, the second is weight, and the third is drag. Since d_n is known, and we have measured the terminal rise velocity of the biofilmed nurdle v_{bf}, we can calculate the biofilm thickness t that is needed. For BF1, which has $v_{bf,BF1} = 4.85 cm/s$, we find that $t = 0.046 mm$. This assumes that the biofilm is distributed evenly along the surface of the nurdle; for the one-sided growth regime of BF1, this would roughly imply a biofilm thickness of $t_{BF1} \approx 0.1 mm$.

We can repeat this analysis for the uniformly biofilmed regime. For N2, $v_{n,N2} = 5.64 cm/s$ which yields $d_{n,N2} = 3.06 mm$. To achieve the measured (reduced) rise velocity of $v_{n,BF2} = 5.35 cm/s$ would require a biofilm thickness of $t_{BF2} = 0.020 mm$, evenly distributed around the

sphere. In other words, the biofilm would need to be approximately five times thicker for the BF1 case than in the BF2 case to explain the measured difference in rise velocities. While our experimental methods cannot directly measure the added mass of the biofilm, a fivefold difference in thickness would have been obvious; this was not observed when we examined the biofilmed nurdles under the microscope as described in the next section. The model implies that the difference in rise velocity cannot be coming from differences in the total amount of biofilm on the nurdles, but must be related to the differences in the spatial distribution of the biofilm.

3.6 Biofilm coverage

To confirm that the nurdles were experiencing equal biofilm growth, and that the difference in rise velocity was not simply caused by BF1 having more added mass than BF2, we compared the biofilm coverage between the two biofilm growth conditions. While we could not directly measure biofilm mass, as discussed in section 3.5, we defined a measurable proxy for the biofilm coverage. As described in section 2.6, we photographed the section of the nurdle qualitatively judged to have the most biofilm under a microscope, in both green light (which caused the biofilm to autofluoresce) and white light (under which the outlines of the opaque black nurdle were clearer). We then used ImageJ to outline the biofilmed area in the green-lit image and the total nurdle area in the white-lit image, defined by intensity thresholding. We define biofilm coverage to be the ratio of area of the biofilm divided by the total in-view area of the nurdle. We qualitatively observed the coverage to be approximately uniform across the entire surface of the nurdle that was exposed to biofilm (one side for BF1 and all sides for BF2). We were not able to perform this analysis for all 50 nurdles per treatment because we were unable to obtain high-quality images for every single nurdle under the microscope; for this analysis, the sample size is reduced to N=34 for BF1 and N=40 for BF2.

Figure 10 shows a histogram of biofilm coverage for BF1 and BF2 and shows that both biofilm growth regimes have similar coverage. We conducted a two-sample t-test to show that the mean biofilm coverage was not significantly different between the two groups ($p = 0.873$). From these results, we conclude that the nearly-identical growing conditions did lead to similar biofilm coverage between the two groups. If anything, this implies that the nurdles in the BF1 treatment had less added mass due to biofilming compared to those in the BF2 treatment (since the biofilm grew only on one side), and yet the rising velocity was reduced more in BF1 than in BF2. The spatial distribution of the biofilm is exclusively driving the difference in observed rising velocity.

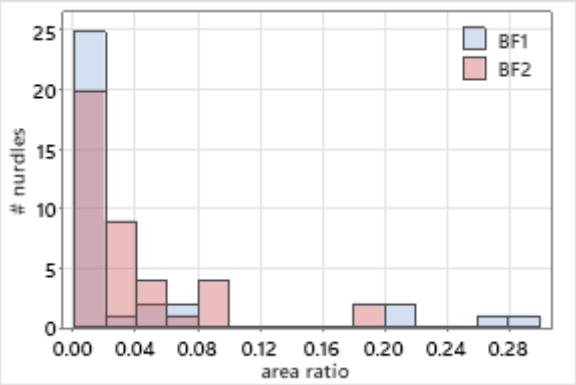

Figure 10. Histograms of ratio of biofilmed area to non-biofilmed area on the surface of a nurdle, used as a proxy for biofilm coverage, for non-uniformly (BF1, N = 34) and uniformly (BF2, N = 40) biofilmed nurdles; difference between the mean area ratio was not significantly different between the two treatments.

3.7 Relationship between biofilm coverage and rise ratio

To conclude our investigation into the effects of biofilm spatial distribution on the rising velocity of microplastic nurdles, we examined the relationship between the rise ratio (see section 3.4) vs. our proxy for biofilm coverage (see section 3.6). We hypothesized that the reduction in rise velocity on a per-nurdle basis would be associated with the amount of biofilm present on the nurdle's surface. Figure 11 shows the nurdle rise ratio *vs.* biofilm coverage for both biofilm growth

regimes (BF1 and BF2). While the exact relationship between these two variables is unclear, we calculated Pearson's correlation coefficient (R) to measure the strength of the linear correlation between the two variables and found it to be equal to -0.292 for BF1 and -0.058 for BF2. This implies that there is a negative correlation between the rise ratio and biofilm coverage, as expected; increased biofilm coverage should result in a reduced rising velocity. The correlation was stronger for BF1 than for BF2, indicating a stronger relationship between rise ratio vs. biofilm coverage for BF1, but both still displayed a negative correlation between the variables. Based on these results, we can conclude that the reduction in rise velocity is associated with the overall amount of biofilm present. However, there is significant variability in both rise velocity and biofilm coverage, without a clear relationship between the two. This is to be expected due to the indirect method of measuring biofilm coverage; however, we can determine that the rise ratio is negatively correlated with the amount of biofilm present, in keeping with the analysis outlined in Section 3.5. A more mechanistic understanding would require more detailed measurements of biofilm coverage.

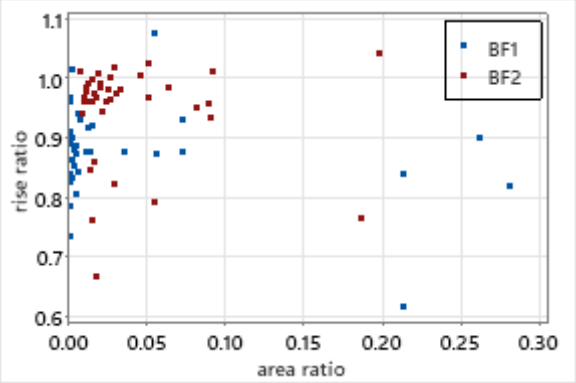

Figure 11. Rise ratio vs. area ratio (representing biofilm coverage) on non-uniformly (BF1, N = 34) and uniformly (BF2, N = 40) biofilmed nurdles; a slight negative correlation was found between the two variables.

A more flexible experimental design along with access to more complex equipment would have allowed us to more robustly characterize the biofilm on the microplastic's surface. One technique that would have given more precise measurements of biofilm coverage is confocal

laser scanning microscopy (CLSM) (Miao et al., 2021). This technique would have allowed us to take multiple images of the biofilm on the surface nurdle at different focal planes. We could then have used image processing to stack the images into one clearly focused image that would have been a 3-dimenstional representation of the biofilm on the surface of the microplastic. This method would have given us a direct measurement of the thickness of the biofilm on the plastic surface of both the BF1 and BF2 treatment groups. A direct measure of the biofilm thickness could have given us a better understanding of how the presence of biofilm affects the rise ratio not only between the two biofilm treatment groups, but across each individual nurdle as well.

Chapter 4: Discussion and Conclusion

In our experiments, we measured the terminal rising velocity, tumbling, and lateral motion of positively buoyant, high-density polyethylene (HDPE) microplastic "nurdles" with and without the presence of biofilm. The plastics were exposed to two different biofilm colonization regimes – non-uniform growth (on a single side of a nurdle) and uniform growth (on all sides of a nurdle). The raw data used to determine the rise velocity and other parameters of interest for the HDPE microplastics as they rose through our rise tank were recorded by two high-speed cameras, positioned orthogonally to one another. We also used a light microscope with epifluorescence to identify and characterize the biofilm that was present on the surface of the microplastics. We used the resulting images to measure a proxy for biofilm coverage (the ratio of biofilmed area to non-biofilmed area). We analyzed these data to understand how the presence and spatial distribution of biofilm affected the rising behavior of the nurdles.

We found that both biofilmed cases (BF1 and BF2) rose more slowly than their non-biofilmed counterparts (N1 and N2). The difference in mean rise velocity was statistically significant at the 95% confidence level between BF1 and the other three groups, and difference in mean rise velocity was statistically significant between BF2 and N2 at the 90% confidence level ($p = 0.054$). Tests of biofilm coverage did not reveal a clear difference between the level of biofilm on the BF1 *vs.* the BF2 nurdles. This implies that two seemingly equally biofilmed nurdles will rise at different rates if the biofilm is colonized on one side of the nurdle rather than uniformly over its surface.

In addition to comparing the overall distribution of the rising velocity between the four treatments, we also examined the percent reduction in rise velocity for each nurdle. We defined a "rise ratio" RR equal to the biofilmed rise velocity divided by the unbiofilmed rise velocity. For

both BF1 and BF2, rise velocity was negatively correlated with our proxy measurement of biofilm coverage, as expected.

From our other measurements, we concluded that the tumbling of the nurdle (proxied by the change in projected area) was not significantly different across the different nurdle treament groups (BF1, BF2, N1, and N2). We conclude that neither the presence nor spatial distribution of biofilm across the nurdle surface affects its tumbling. It is unlikely that the tumbling of the nurdles accounts for the reduction in rise velocity between the different biofilm treatment groups. However, our measurements of lateral motion (the standard deviation of the nurdles' horizontal (x) position) revealed a significant difference between BF1 and the other three groups. A difference in mean lateral motion was not statistically significant between BF2 and N2 ($p = 0.367$). From these results, we conclude that biofilm distribution affects the lateral motion of differently biofilmed nurdles. In other words, when the biofilm is concentrated on a single side of a nurdle, there is more side-to-side motion. This lowers the overall rise velocity, as it increases the frictional drag on the nurdle. However, we do not yet understand the physical mechanisms driving this motion.

Our major conclusion is that the spatial distribution of a biofilm on the surface of a microplastic particle impacts its overall settling or rising velocity. This has major implications for the fate of microplastics within the environment. Given that most microplastics are positively buoyant and float until enough biofilm develops upon their surface to induce sinking (Amaral-Zettler et al., 2021), it is likely that the initial biofilms develop on their submerged side. Our work shows that this uneven development of biofilm can alter the settling or rising velocity of microplastics in unexpected ways, and that a spatially non-uniform biofilm cannot be approximated as a uniform addition of mass distributed around the particle. In a natural environment, a microplastic may not remain in a consistent orientation as in our experiments, but depending on the shape of the particle it may have a preferred orientation at the surface or in the water column. A buoyant microplastic with a non-uniform biofilm on the submerged side could eventually grow

additional biofilm that may make it permanently submerge (Ye & Andrady, 1991). For these and other weakly positively or negatively buoyant plastics, differences in the availability of light between the top and the bottom of the particle are likely to lead to differences in biofilm development, and the subsequent non-uniform distribution of added mass. This non-uniform distribution, as we have shown, is likely to lead to changes in the settling or rising velocity in ways that are not well-addressed by existing models, which often assume uniform coverage (Mendrik et al., 2022; Miao et al., 2021; Semcesen & Wells, 2021). The mechanism by which the rising velocity is altered is unclear; we hypothesize that the frictional drag on the particle may be uneven from the biofilmed side to the non-biofilmed side, as the biofilmed side is effectively covered with a porous surface that may lead to a semi-slip boundary (while the non-biofilmed side maintains a no-slip boundary). Further studies are needed to clarify how biofilmed particles experience drag and fluid shear at their surface, and how this may alter the overall settling of a biofilmed *vs.* unbiofilmed particle as well as how it may manifest in a particle with an uneven distribution of biofilm.

We also showed in our experiments that microplastics with a non-uniform biofilm experience a larger variability in their lateral motion. This may increase collisions and promote aggregation (Michels et al., 2018); an increased aggregation rate may alter the vertical distribution of microplastics, and increase the fraction of microplastics that sink to the ocean floor where they may be ingested by organisms or buried in sediment(Carson, 2013; Savoca et al., 2017). This change in vertical distribution may also increase contact with calcareous fouling organisms such as barnacles and mussels, which are likely to further increase the overall mass density of the microplastics so that even highly positively buoyant plastics become permanently submerged below the water surface (Kaiser et al., 2017). The increase in lateral motion from non-uniformly distributed biofilm may also affect overall transport, shifting our models of how microplastics move within the environment at large(López et al., 2021) .

Future experiments may benefit from a more robust way of characterizing the amount of biofilm on the surface of microplastics. Our experiments were limited in their ability to characterize biofilm coverage; more complex methods such as confocal microscopy or various forms of spectroscopy may have given more information, but testing would have interfered with our ability to directly measure the rising velocity. However, a larger sample size and more flexible experimental design could provide other avenues for characterizing and quantifying biofilm coverage.

Another future avenue to extend this work would be to compare the settling behavior of different kinds of microplastics exposed to even more biofilm colonization regimes. Within the natural environment, there exist flows that can affect the biofilm architecture as it grows on the surface of a microplastic. A microplastic growing in still water is more likely to develop a biofilm that is fluffy and less dense than a biofilm that would develop on a microplastic exposed to flowing water, as in a river or stream (Araújo et al., 2016; Fanesi et al., 2021). Comparing more biofilm colonization regimes could to a more nuanced understanding of how different mass distributions on the surface of a microplastic affect overall settling behavior. Finally, turbulence is a common state of environmental flows in which microplastics are found. Another future direction for this work would be to subject microplastics with different biofilm mass distributions to turbulent flow and compare their behavior.

While our experiments compare microplastics subjected to only two colonization regimes in still water, this simple experiment still showed significant differences in microplastic behavior based on the spatial distribution of biofilm. There are still many ways to expand our work and discover even more about how biofilms affect the settling behavior of microplastics.

References

Abelev, A. v., Valent, P. J., & Holland, K. T. (2007). Behavior of a large cylinder in free-fall through water. *IEEE Journal of Oceanic Engineering*, *32*(1), 10–20. https://doi.org/10.1109/JOE.2007.890938

Amaral-Zettler, L. A., Zettler, E. R., Mincer, T. J., Klaassen, M. A., & Gallager, S. M. (2021). Biofouling impacts on polyethylene density and sinking in coastal waters: A macro/micro tipping point? *Water Research*, *201*. https://doi.org/10.1016/J.WATRES.2021.117289

Andrady, A. L. (2011). Microplastics in the marine environment. *Marine Pollution Bulletin*, *62*(8), 1596–1605. https://doi.org/10.1016/J.MARPOLBUL.2011.05.030

Andrady, A. L. (2017). The plastic in microplastics: A review. *Marine Pollution Bulletin*, *119*(1), 12–22. https://doi.org/10.1016/J.MARPOLBUL.2017.01.082

Angle, B. R., Rau, M. J., & Byron, M. L. (2019). Effect of mass distribution on falling cylindrical particles at intermediate Reynolds numbers. *Volume 5: Multiphase Flow*. https://doi.org/10.1115/ajkfluids2019-5458

Araújo, P. A., Malheiro, J., Machado, I., Mergulhão, F., Melo, L., & Simões, M. (2016). Influence of Flow Velocity on the Characteristics of Pseudomonas fluorescens Biofilms . *Journal of Environmental Engineering*, *142*(7), 04016031. https://doi.org/10.1061/(ASCE)EE.1943-7870.0001068

Arndt, H., Schmidt-Denter, K., Auer, B., & Weitere, M. (2003). Protozoans and Biofilms. *Fossil and Recent Biofilms*, 161–179. https://doi.org/10.1007/978-94-017-0193-8_10

Auta, H. S., Emenike, C. U., Jayanthi, B., & Fauziah, S. H. (2018). Growth kinetics and biodeterioration of polypropylene microplastics by Bacillus sp. and Rhodococcus sp. isolated

from mangrove sediment. *Marine Pollution Bulletin*, *127*, 15–21. https://doi.org/10.1016/J.MARPOLBUL.2017.11.036

Carson, H. S. (2013). The incidence of plastic ingestion by fishes: From the prey's perspective. *Marine Pollution Bulletin*, *74*(1), 170–174. https://doi.org/10.1016/J.MARPOLBUL.2013.07.008

Caruso, G. (2019). Microplastics as vectors of contaminants. *Marine Pollution Bulletin*, *146*, 921–924. https://doi.org/10.1016/J.MARPOLBUL.2019.07.052

Cashman, M. A., Langknecht, T., el Khatib, D., Burgess, R. M., Boving, T. B., Robinson, S., & Ho, K. T. (2022). Quantification of microplastics in sediments from Narragansett Bay, Rhode Island USA using a novel isolation and extraction method. *Marine Pollution Bulletin*, *174*. https://doi.org/10.1016/J.MARPOLBUL.2021.113254

Cau, A., Carlo, ⊥, Avio, G., Dessì, C., Moccia, D., Pusceddu, A., Regoli, F., Cannas, R., & Follesa, M. C. (2020). Benthic Crustacean Digestion Can Modulate the Environmental Fate of Microplastics in the Deep Sea. *Environ. Sci. Technol*, *54*, 4892. https://doi.org/10.1021/acs.est.9b07705

Chae, Y., & An, Y. J. (2018). Current research trends on plastic pollution and ecological impacts on the soil ecosystem: A review. *Environmental Pollution*, *240*, 387–395. https://doi.org/10.1016/J.ENVPOL.2018.05.008

Chen, X., Xiong, X., Jiang, X., Shi, H., & Wu, C. (2019). Sinking of floating plastic debris caused by biofilm development in a freshwater lake. *Chemosphere*, *222*, 856–864. https://doi.org/10.1016/J.CHEMOSPHERE.2019.02.015

Chu, J. L., Gilles, A. F., Fan, C. W., Lan, J., Chu, P. C., Gilles, A. F., Fan, C., Lan, J., & Fleischer, P. (2002). Hydrodynamics Of Falling Cylinder in Water Column. *Advances in Fluid Mechanics*. http://hdl.handle.net/10945/36309

Clift, R. (1970). The motion of particles in turbulent gas-streams. *Proc. Chemeca'70*, *1*, 14.

Costa, P. J. M. (2016). Sediment Transport. *Encyclopedia of Earth Sciences Series*, 562–567. https://doi.org/10.1007/978-94-017-8801-4_187

Cox, K. D., Covernton, G. A., Davies, H. L., Dower, J. F., Juanes, F., & Dudas, S. E. (2019). Human consumption of microplastics. *Environmental Science & Technology*, 53(12), 7068–7074. https://doi.org/10.1021/acs.est.9b01517

Crouzet, M., Le Senechal, C., Brözel, V. S., Costaglioli, P., Barthe, C., Bonneu, M., Garbay, B., & Vilain, S. (2014). Exploring early steps in biofilm formation: Set-up of an experimental system for molecular studies. *BMC Microbiology*, 14(1). https://doi.org/10.1186/s12866-014-0253-z

Čulin, J., & Bielić, T. (2016). Plastic Pollution from Ships. *Journal of Maritime & Transportation Science*, *51*(1), 57–66. https://doi.org/10.18048/2016.51.04

Dauvergne, P. (2018). The power of environmental norms: Marine Plastic Pollution and the politics of microbeads. Environmental Politics, 27(4), 579–597. https://doi.org/10.1080/09644016.2018.1449090

Dawson, A. L., Kawaguchi, S., King, C. K., Townsend, K. A., King, R., Huston, W. M., & Bengtson Nash, S. M. (2018). Turning microplastics into nanoplastics through digestive fragmentation by Antarctic krill. *Nature Communications*. https://doi.org/10.1038/s41467-018-03465-9

Donlan, R. M. (2001). Biofilm Formation: A Clinically Relevant Microbiological Process. *Clinical Infectious Diseases*, *33*, 1387–1392. https://academic.oup.com/cid/article/33/8/1387/347551

Donlan, R. M. (2002). Biofilms: Microbial Life on Surfaces. *Emerging Infectious Diseases* •, *8*(9). http://www.microbelibrary.org/

Duan, J., Bolan, N., Li, Y., Ding, S., Atugoda, T., Vithanage, M., Sarkar, B., Tsang, D. C. W., & Kirkham, M. B. (2021). Weathering of microplastics and interaction with other coexisting constituents in terrestrial and aquatic environments. *Water Research*, *196*, 117011. https://doi.org/10.1016/j.watres.2021.117011

Enfrin, M., Lee, J., Gibert, Y., Basheer, F., Kong, L., & Dumée, L. F. (2020). Release of hazardous nanoplastic contaminants due to microplastics fragmentation under shear stress forces. *Journal of Hazardous Materials*, *384*. https://doi.org/10.1016/J.JHAZMAT.2019.121393

Fabra, M., Williams, L., Watts, J. E. M., Hale, M. S., Couceiro, F., & Preston, J. (2021). The plastic trojan horse: Biofilms increase microplastic uptake in marine filter feeders impacting microbial transfer and Organism Health. *Science of The Total Environment*, 797, 149217. https://doi.org/10.1016/j.scitotenv.2021.149217

Fanesi, A., Lavayssière, M., Breton, C., Bernard, O., Briandet, R., & Lopes, F. (2021). Shear stress affects the architecture and cohesion of Chlorella vulgaris biofilms. *Scientific Reports 2021 11:1*, *11*(1), 1–11. https://doi.org/10.1038/s41598-021-83523-3

Frère, L., Maignien, L., Chalopin, M., Huvet, A., Rinnert, E., Morrison, H., Kerninon, S., Cassone, A. L., Lambert, C., Reveillaud, J., & Paul-Pont, I. (2018). Microplastic bacterial communities in the Bay of Brest: Influence of polymer type and size. *Environmental Pollution*, *242*, 614–625. https://doi.org/10.1016/J.ENVPOL.2018.07.023

Froelich, B. A., Williams, T. C., Noble, R. T., & Oliver, J. D. (2012). Apparent Loss of Vibrio vulnificus from North Carolina Oysters Coincides with a Drought-Induced Increase in Salinity. *Applied and Environmental Microbiology*, *78*(11), 3885. https://doi.org/10.1128/AEM.07855-11

Garrett, T. R., Bhakoo, M., & Zhang, Z. (2008). Bacterial adhesion and biofilms on surfaces. *Progress in Natural Science*, *18*(9), 1049–1056. https://doi.org/10.1016/J.PNSC.2008.04.001

Guan, J., Qi, K., Wang, J., Wang, W., Wang, Z., Lu, N., & Qu, J. (2020). Microplastics as an emerging anthropogenic vector of trace metals in freshwater: Significance of biofilms and comparison with natural substrates. *Water Research*, *184*. https://doi.org/10.1016/J.WATRES.2020.116205

Harrison, J. P., Hoellein, T. J., Sapp, M., Tagg, A. S., Ju-Nam, Y., & Ojeda, J. J. (2018). Microplastic-associated biofilms: A comparison of freshwater and marine environments. The Handbook of Environmental Chemistry, 181–201. https://doi.org/10.1007/978-3-319-61615-5_9

Heithoff, D. M., & Mahan, M. J. (2004). Vibrio Cholerae Biofilms: Stuck between a rock and a hard place. Journal of Bacteriology, 186(15), 4835–4837. https://doi.org/10.1128/jb.186.15.4835-4837.2004

Horton, A. A., & Dixon, S. J. (2018). Microplastics: An introduction to environmental transport processes. *WIREs Water*, *5*(2). https://doi.org/10.1002/WAT2.1268

Jiang, C., Yin, L., Wen, X., Du, C., Wu, L., Long, Y., Liu, Y., Ma, Y., Yin, Q., Zhou, Z., & Pan, H. (2018). Microplastics in Sediment and Surface Water of West Dongting Lake and South Dongting Lake: Abundance, Source and Composition. *International Journal of Environmental Research and Public Health*, *15*(10). https://doi.org/10.3390/IJERPH15102164

Johnson, A. C., Ball, H., Cross, R., Horton, A. A., Jürgens, M. D., Read, D. S., Vollertsen, J., & Svendsen, C. (2020). Identification and quantification of microplastics in potable water and their sources within Water Treatment Works in England and Wales. *Environmental Science & Technology*, *54*(19), 12326–12334. https://doi.org/10.1021/acs.est.0c03211

Kaiser, D., Kowalski, N., & Waniek, J. J. (2017). Effects of biofouling on the sinking behavior of microplastics. *Environmental Research Letters*, *12*(12), 124003. https://doi.org/10.1088/1748-9326/AA8E8B

Kernien, J. F., Snarr, B. D., Sheppard, D. C., & Nett, J. E. (2018). The interface between fungal biofilms and innate immunity. *Frontiers in Immunology*, *8*(Jan), 1968. https://doi.org/10.3389/FIMMU.2017.01968/BIBTEX

Koelmans, A. A., Mohamed Nor, N. H., Hermsen, E., Kooi, M., Mintenig, S. M., & de France, J. (2019a). Microplastics in freshwaters and drinking water: Critical review and assessment of data quality. *Water Research*, *155*, 410–422. https://doi.org/10.1016/J.WATRES.2019.02.054

Koelmans, A. A., Mohamed Nor, N. H., Hermsen, E., Kooi, M., Mintenig, S. M., & de France, J. (2019b). Microplastics in freshwaters and drinking water: Critical review and assessment of data quality. *Water Research*, *155*, 410–422. https://doi.org/10.1016/J.WATRES.2019.02.054

Kostakioti, M., Hadjifrangiskou, M., & Hultgren, S. J. (2013). Bacterial Biofilms: Development, Dispersal, and Therapeutic Strategies in the Dawn of the Postantibiotic Era. *Cold Spring Harbor Perspectives in Medicine*, *3*(4). https://doi.org/10.1101/CSHPERSPECT.A010306

Kowalski, N., Reichardt, A. M., & Waniek, J. J. (2016). Sinking rates of microplastics and potential implications of their alteration by physical, biological, and chemical factors. *Marine Pollution Bulletin*, *109*(1), 310–319. https://doi.org/10.1016/J.MARPOLBUL.2016.05.064

Lagarde, F., Olivier, O., Zanella, M., Daniel, P., Hiard, S., & Caruso, A. (2016). Microplastic interactions with freshwater microalgae: Hetero-aggregation and changes in plastic density appear strongly dependent on polymer type. *Environmental Pollution*, *215*, 331–339. https://doi.org/10.1016/J.ENVPOL.2016.05.006

Lehtola, M. J., Laxander, M., Miettinen, I. T., Hirvonen, A., Vartiainen, T., & Martikainen, P. J. (2006). The effects of changing water flow velocity on the formation of biofilms and water quality in pilot distribution system consisting of copper or polyethylene pipes. *Water Research*, *40*(11), 2151–2160. https://doi.org/10.1016/J.WATRES.2006.04.010

Leiser, R., Schumann, M., Dadi, T., & Wendt-Potthoff, K. (2021). Burial of microplastics in freshwater sediments facilitated by iron-organo flocs. *Scientific Reports*, *11*(24072). https://doi.org/10.1038/s41598-021-02748-4

Li, W. C., Tse, H. F., & Fok, L. (2016). Plastic waste in the marine environment: A review of sources, occurrence, and effects. *Science of The Total Environment*, *566–567*, 333–349. https://doi.org/10.1016/J.SCITOTENV.2016.05.084

Li, W., Zhang, Y., Wu, N., Zhao, Z., Xu, W., Ma, Y., & Niu, Z. (2019). Colonization characteristics of bacterial communities on plastic debris influenced by environmental factors and polymer types in the Haihe estuary of Bohai Bay, China. *Environmental Science & Technology*, 53(18), 10763–10773. https://doi.org/10.1021/acs.est.9b03659

Li, Y., Sun, Y., Li, J., Tang, R., Miu, Y., & Ma, X. (2021). Research on the influence of microplastics on Marine Life. *IOP Conference Series: Earth and Environmental Science, 631*(1), 012006. https://doi.org/10.1088/1755-1315/631/1/012006

Lindeque, P. K., Cole, M., Coppock, R. L., Lewis, C. N., Miller, R. Z., Watts, A. J. R., Wilson-McNeal, A., Wright, S. L., & Galloway, T. S. (2020). Are we underestimating microplastic abundance in the marine environment? A comparison of microplastic capture with nets of different mesh-size. *Environmental Pollution*, *265*, 114721. https://doi.org/10.1016/J.ENVPOL.2020.114721

Liu, J., Liang, J., Ding, J., Zhang, G., Zeng, X., Yang, Q., Zhu, B., & Gao, W. (2021). Microfiber pollution: an ongoing major environmental issue related to the sustainable development of textile and clothing industry. *Environment, Development and Sustainability*, *23*(8), 11240–11256. https://doi.org/10.1007/S10668-020-01173-3/FIGURES/2

Long, M., Moriceau, B., Gallinari, M., Lambert, C., Huvet, A., Raffray, J., & Soudant, P. (2015). Interactions between microplastics and phytoplankton aggregates: Impact on their respective fates. *Marine Chemistry*, *175*, 39–46. https://doi.org/10.1016/J.MARCHEM.2015.04.003

López, A. G., Najjar, R. G., Friedrichs, M. A. M., Hickner, M. A., & Wardrop, D. H. (2021). Estuaries as Filters for Riverine Microplastics: Simulations in a Large, Coastal-Plain Estuary. *Frontiers in Marine Science*, *8*. https://doi.org/10.3389/FMARS.2021.715924

Manuel, C. M., Nunes, O. C., & Melo, L. F. (2007). Dynamics of drinking water biofilm in flow/non-flow conditions. *Water Research*, *41*(3), 551–562. https://doi.org/10.1016/J.WATRES.2006.11.007

Mendrik, F., Fernández, R., Waller, C., Hackney, C., & Parsons, D. (2022). Shifting settling regimes of aquatic microplastics, *ArXiv* . https://doi.org/10.21203/RS.3.RS-1498318/V1

Miao, L., Gao, Y., Adyel, T. M., Huo, Z., Liu, Z., Wu, J., & Hou, J. (2021). Effects of biofilm colonization on the sinking of microplastics in three freshwater environments. *Journal of Hazardous Materials*, *413*. https://doi.org/10.1016/J.JHAZMAT.2021.125370

Miao, L., Wang, P., Hou, J., Yao, Y., Liu, Z., Liu, S., & Li, T. (2019). Distinct community structure and microbial functions of biofilms colonizing microplastics. *Science of The Total Environment*, *650*, 2395–2402. https://doi.org/10.1016/J.SCITOTENV.2018.09.378

Michels, J., Stippkugel, A., Lenz, M., Wirtz, K., & Engel, A. (2018). Rapid aggregation of biofilm-covered microplastics with marine biogenic particles. *The Royal Society*. https://doi.org/10.1098/rspb.2018.1203

Novotna, K., Cermakova, L., Pivokonska, L., Cajthaml, T., & Pivokonsky, M. (2019). Microplastics in drinking water treatment – Current knowledge and research needs. *Science of the Total Environment*, *667*, 730–740. https://doi.org/10.1016/J.SCITOTENV.2019.02.431

Oberbeckmann, S., Kreikemeyer, B., & Labrenz, M. (2018). Environmental factors support the formation of specific bacterial assemblages on microplastics. *Frontiers in Microbiology*, *8*(Jan). https://doi.org/10.3389/FMICB.2017.02709/FULL

Park, A., Jeong, H. H., Lee, J., Kim, K. P., & Lee, C. S. (2011). Effect of shear stress on the formation of bacterial biofilm in a microfluidic channel. *BioChip Journal 2011 5:3*, *5*(3), 236–241. https://doi.org/10.1007/S13206-011-5307-9

Pastorino, P., Prearo, M., Pizzul, E., Elia, A. C., Renzi, M., Ginebreda, A., & Barceló, D. (2022). High-mountain lakes as indicators of microplastic pollution: current and future perspectives. *Water Emerg Contam Nanoplastics*. https://doi.org/10.20517/wecn.2022.01

Pham, D. N., Clark, L., & Li, M. (2021). Microplastics as hubs enriching antibiotic-resistant bacteria and pathogens in municipal activated sludge. *Journal of Hazardous Materials Letters*, *2*. https://doi.org/10.1016/J.HAZL.2021.100014

Pinnell, L. J., & Turner, J. W. (2020). Temporal changes in water temperature and salinity drive the formation of a reversible plastic-specific microbial community. *FEMS Microbiology Ecology*, *96*(12), 230. https://doi.org/10.1093/FEMSEC/FIAA230

Pinto, M., Langer, T. M., Hüffer, T., Hofmann, T., & Herndl, G. J. (2019). The composition of bacterial communities associated with plastic biofilms differs between different polymers and stages of biofilm succession. *PLOS ONE*, *14*(6). https://doi.org/10.1371/journal.pone.0217165

Pohl, F., Eggenhuisen, J. T., Kane, I. A., & Clare, M. A. (2020). Transport and Burial of Microplastics in Deep-Marine Sediments by Turbidity Currents. *Environ. Sci. Technol*, *54*, 4180–4189. https://doi.org/10.1021/acs.est.9b07527

Richard, H., Carpenter, E. J., Komada, T., Palmer, P. T., & Rochman, C. M. (2019). Biofilm facilitates metal accumulation onto microplastics in estuarine waters. *Science of the Total Environment*, *683*, 600–608. https://doi.org/10.1016/J.SCITOTENV.2019.04.331

Saha, M., Naik, A., Desai, A., Nanajkar, M., Rathore, C., Kumar, M., & Gupta, P. (2021). Microplastics in seafood as an emerging threat to marine environment: A case study in Goa, west coast of India. *Chemosphere*, *270*. https://doi.org/10.1016/J.CHEMOSPHERE.2020.129359

Savoca, M. S., Tyson, C. W., Mcgill, M., & Slager, C. J. (2017). Odours from marine plastic debris induce food search behaviours in a forage fish. *Royal Society*. https://doi.org/10.1098/rspb.2017.1000

Semcesen, P. O., & Wells, M. G. (2021a). Biofilm growth on buoyant microplastics leads to changes in settling rates: Implications for microplastic retention in the Great Lakes. *Marine Pollution Bulletin*, *170*. https://doi.org/10.1016/J.MARPOLBUL.2021.112573

Stefánsson, H., Peternell, M., Konrad-Schmolke, M., Hannesdóttir, H., Ásbjörnsson, E. J., & Sturkell, E. (2021). Microplastics in glaciers: First results from the vatnajökull ice cap. *Sustainability (Switzerland)*, *13*(8). https://doi.org/10.3390/SU13084183

Stenger, K. S., Wikmark, O. G., Bezuidenhout, C. C., & Molale-Tom, L. G. (2021). Microplastics pollution in the ocean: Potential carrier of resistant bacteria and resistance genes. *Environmental Pollution*, *291*, 118130. https://doi.org/10.1016/J.ENVPOL.2021.118130

Thapa, S., Bharti, A., & Prasanna, R. (2017). Algal Biofilms and Their Biotechnological Significance. *Algal Green Chemistry: Recent Progress in Biotechnology*, 285–303. https://doi.org/10.1016/B978-0-444-63784-0.00014-X

Thompson, R. C., Olsen, Y., Mitchell, R. P., Davis, A., Rowland, S. J., John, A. W. G., Mcgonigle, D., & Russell, A. E. (2004). Lost at Sea: Where Is All the Plastic? *Science*, *304*(5672). https://doi.org/10.1126/science.1094559

Tu, C., Zhou, Q., Zhang, C., Liu, Y., & Luo, Y. (2020). Biofilms of Microplastics. *Handbook of Environmental Chemistry*, *95*, 299–317. https://doi.org/10.1007/698_2020_461/TABLES/1

Vasudevan, R. (2014). Biofilms: Microbial Cities of Scientific Significance. *Journal of Microbiology & Experimentation*, *1*(3). https://doi.org/10.15406/JMEN.2014.01.00014

Waldschläger, K., & Schüttrumpf, H. (2019). Effects of particle properties on the settling and rise velocities of microplastics in freshwater under laboratory conditions. *Environmental Science & Technology*, 53(4), 1958–1966. https://doi.org/10.1021/acs.est.8b06794

Wang, J., Guo, X., & Xue, J. (2021). Biofilm-Developed Microplastics as Vectors of Pollutants in Aquatic Environments. *Environ. Sci. Technol*, *55*. https://doi.org/10.1021/acs.est.1c04466

Wang, J., Lu, J., Zhang, Y., Wu, J., & Luo, Y. (2021). Unique Bacterial Community of the Biofilm on Microplastics in Coastal Water. *Bulletin of Environmental Contamination and Toxicology*, *107*(4), 597–601. https://doi.org/10.1007/S00128-020-02875-0/FIGURES/4

Wang, Y., Wang, X., Li, Y., Li, J., Liu, Y., Xia, S., & Zhao, J. (2021). Effects of exposure of polyethylene microplastics to air, water, and soil on their adsorption behaviors for copper and tetracycline. *Chemical Engineering Journal*, *404*. https://doi.org/10.1016/J.CEJ.2020.126412

Wäsche, S., Horn, H., & Hempel, D. C. (2002). Influence of growth conditions on biofilm development and mass transfer at the bulk/biofilm interface. *Water Research*, *36*(19), 4775–4784. https://doi.org/10.1016/s0043-1354(02)00215-4

Will, J. B., & Krug, D. (2021). Rising and Sinking in Resonance: Mass Distribution Critically Affects Buoyancy-Driven Spheres via Rotational Dynamics. *Physical Review Letters*, *126*, 174502. https://doi.org/10.1103/PhysRevLett.126.174502

Wu, X., Pan, J., Li, M., Li, Y., Bartlam, M., & Wang, Y. (2019). Selective enrichment of bacterial pathogens by microplastic biofilm. *Water Research*, *165*, 114979. https://doi.org/10.1016/J.WATRES.2019.114979

Ye, S., & Andrady, A. L. (1991). Fouling of floating plastic debris under Biscayne Bay exposure conditions. *Marine Pollution Bulletin*, *22*(12), 608–613. https://doi.org/10.1016/0025-326X(91)90249-R

Yousif, E., & Haddad, R. (2013). Photodegradation and photostabilization of polymers, especially polystyrene: *Review*. *SpringerPlus*, *2*(1). https://doi.org/10.1186/2193-1801-2-398

Ziccardi, L. M., Edgington, A., Hentz, K., Kulacki, K. J., & Kane Driscoll, S. (2016). Microplastics as vectors for bioaccumulation of hydrophobic organic chemicals in the marine environment: A state-of-the-science review. *Environmental Toxicology and Chemistry*, *35*(7), 1667–1676. https://doi.org/10.1002/ETC.3461

Appendix A

Biofilm Growth and Characterization Procedure

Biofilm Growth Procedure

The same steps were completed for each strain of bacteria that was prepared to maintain consistency between growth in each flask. The full list of procedural steps are listed in chronological order.

1. Throughly clean the Erlenmeyer flasks in preparation for culture medium. Rinse several times, then soak in hot water for a final rinse.
2. Using a 500 mL Erlenmeyer flask, fill the flask to approximately 150 mL with freshly prepared media and sterilize the media (autoclave for 20 minutes at 121°C and 15 psi). Allow the media to cool overnight before adding any algae. Repeat the process for the other flasks and media.
3. Add a small amount (2–5 mL) of inoculum from the culture provided, handling both containers in a sterile manner.
4. Thoroughly clean the microplastic nurdle samples to be introduced to the inoculum. Rinse several times, then soak in hot water for a final rinse.
5. Carefully introduce the cleaned Microplastics to the Erlenmeyer flasks by dropping them through the mouth of the flask with a pair of tweezers. Add about 20 samples to each flask.
6. Screw the caps on each of the Erlenmeyer flasks so that they each one is tightly sealed.

7. Label each of the samples with a piece of tape indicating the cell line type (type of bacteria), passage number (number of times the cell has been subcultured), date, and initials.

8. Place the flasks under the controlled 12H/12H light source and allow culture growth for 9 weeks, monitor the growth on samples every two weeks by looking at bacterial growth under the microscope.
9. Remove several microplastic samples and place in a Petri dish for viewing under the microscope to confirm growth on the samples.

Biofilm Characterization Procedure

The same steps were completed for each nurdle that was looked at under the microscope to maintain consistency between all images. The full list of procedural steps are listed in chronological order.

1. Calibrate microscope view using micrometer slide.
2. Place biofilm-developed nurdle on slide.
3. Illuminate with green light.
4. Place nurdle in orientation where maximum biofilm coverage is visible.
5. Take photo and store with appropriate file name.
6. Illuminate the nurdle with white light and take an additional photo, store with appropriate file name. (For later identification of nurdle edges if necessary)

Appendix B

Primary Variable Processing Codes

This code converts the individual frames from each high-speed camera video into a binary image. Next, the centroid position of the nurdle, the change in the nurdle's area with respect to time, and the nurdle's change in perimeter with respect to time is recorded for both high speed cameras into data structures.

```
% Track position of nurdle
clear; clc;

s = dir('*.mat')); %Loads all the .mat files present in the
current directory
files = {s.name}; %Stores the files in workspace
for k = 1:numel(files)
   clearvars -except s files k BF1_C1_17
   load(files{k}) %Loads file '#k' from workspace
   [a b c]=size(F); %determines size of file where a and b are
   resolution and c is the frame
                              %number in the sequence

   % Finds the nurdle for the entire sequence.
   clc;
   se = strel('disk',4,8);

   %Starts at a later frame to ensure that full nurdle is in view
   for e = 1:c %Loop through all frames
       Im = F(:,:,e); %Identify current frame images
       NurdEdge = edge(Im,'canny',[0.1 0.8]); %Find edges of
nurdle
       Nurd(:,:,e) = bwconvhull(NurdEdge,'objects'); %close the
edges so there are no open lines
                                          %without the dependence
of picking a size

%for structuring elements
       Nurd(:,:,e) = imfill(Nurd(:,:,e),'holes'); %fill any
cutouts left in the blob
```

```
       %First attempt to remove objects that are not the nurdle
       Nurd(:,:,e) = bwlabel(Nurd(:,:,e), 8); % Label each blob
so we can make measurements of
                                    % it
       all_data = regionprops(Nurd(:,:,e),'all'); %Get geometric
properties of all blobs in the frame
       allBlobCir = [all_data.Circularity]; %Circularity of each
blob in the frame (Perfect circle
                                 %has circularity of 1)
       allBlobArea = [all_data.Area]; %Area of each of the blobs
in the frame
       allowableCirIndexes = allBlobCir < 1.1;  %Filters out
blobs that have a circluarity greater
                                              %than 1.1
       AllowableCirIndexes = allBlobCir > 0.8;   %Filters out
blobs that have a circularity less
                                           %than 0.8
       allowableAreaIndexes = allBlobArea > 500; %Filters out
blobs that have an area >300p^2
       keeperIndexes = find(allowableCirIndexes &
AllowableCirIndexes & …
                            allowableAreaIndexes); %Finds the idexes
of the blobs that meet the
                                             %above criterion
       keeperBlobsImage = ismember(Nurd(:,:,e), keeperIndexes);%
Extract only those blobs that
                                                    % meet our
criteria, and
                                                    %eliminate those
blobs that
                                                    %don't meet our
criteria.
       Nurd(:,:,e) = bwlabel(keeperBlobsImage, 8); %Nurd(:,:,e)
is now a black and white image
                                           %with a white blob where
the nurdle was.

       % Second check that only nurdle is in frame just in case
there is a
       % blob that meets all the parameters that are defined
above
       Nurd = double(Nurd); %convert the logical Nurd var into a
double
       if max(max(bwlabel(Nurd(:,:,e))))>1 ||
max(max(bwlabel(Nurd(:,:,e))))<1…

Nurd(:,:,e)=nan(size(Nurd(:,:,e)));
           Area(e) = nan;
           Perimeter(e) = nan;
           centroidsX(e) = nan;
```

```
            centroidsY(e) = nan;
            continue
        end

        all_data = regionprops(Nurd(:,:,e),'all'); %Get geometric
properties of nurdle

        Pos = [all_data.Centroid]; %Find nurdle centroid (for
tracking)
        Area(e) = [all_data.Area]; %Find projected area of nurdle
        Perimeter(e) = [all_data.Perimeter]; %Find perimeter of
projected area


        centroidsX(e)=Pos(1); %Store the x-coordinate of the
nurdle centroid
        centroidsY(e)=Pos(2); %Store y-coordinate of nurdle
centroid


    end

    % Position, Area, and Perimeter calculations
    clc; close all;
    calib = 104.69; %pixels to cm conversion rate determined from
calibration image

    Area=Area*((1/calib)^2); %convert pixels^2 to cm^2

    Perimeter=Perimeter*(1/calib); %convert pixels to cm

    % Velocity calculation with Central Differencing Scheme
    y=centroidsY.*(1/calib); %convert pixels to cm
    dt = 0.002; %total time which is frames at 500 fps or 2ms
    posy = diff(y(1:end-1))+diff(y(2:end)); %gives delta y for
central differencing
    vel = posy*(1/(2*dt)); %central difference to calculate the
velocity in the y-direction

    x=centroidsX.*(1/calib); %convert pixels to cm

    % Data Structure array to store primary data
    BF1_C1_17(k).A=Area;
    BF1_C1_17(k).P=Perimeter;
    BF1_C1_17(k).XPos=x;
    BF1_C1_17(k).YPos=y;
    BF1_C1_17(k).V=vel;

    save('BF1_C1_17.mat','BF1_C1_17','-v7.3')
end
```

Synchronization code

This code is used to synchronize the time series of the data structures containing nurdle area, perimeter, x-position, y-position, and velocity and removes the NaN values that were entered into the data structures for when the nurdle was not within the FOV at the beginning and end of the videos. It returns the final data structures used for analysis.

```
%Synchronize the times series within the data structures
clc, clear, close all
load('BF1_nans.mat')%loads in the desired set of data to be
sychronized

for j =1:length(BF1_nans)
    clearvars -except BF1_nans BF1 j
    %Create "NaN locators" of zeros and ones (ones where NaNs
are, zeros
    %where numbers are)
    AC1 = double(isnan(BF1_nans(1,j).A)); %identifies which
elements of the array are NaNs and
                                %converts the logical array into
                            and an array of
                                %double precision values
    AC2 = double(isnan(BF1_nans(2,j).A)); %identifies which
elements of the array are NaNs and
                                %converts the logical array into
                            and an array of
                                %double precision values
    PC1 = double(isnan(BF1_nans(1,j).P)); %identifies which
elements of the array are NaNs and converts the logical array
into and an array of double precision values
    PC2 = double(isnan(BF1_nans(2,j).P)); %identifies which
elements of the array are NaNs and converts the logical array
into and an array of double precision values
    XC1 = double(isnan(BF1_nans(1,j).XPos)); %identifies which
elements of the array are NaNs and converts the logical array
into and an array of double precision values
    XC2 = double(isnan(BF1_nans(2,j).XPos)); %identifies which
elements of the array are NaNs and converts the logical array
into and an array of double precision values
    YC1 = double(isnan(BF1_nans(1,j).YPos)); %identifies which
elements of the array are NaNs
                                    %and converts the logical
                            array into and an array
                                    %of double precision values
    YC2 = double(isnan(BF1_nans(2,j).YPos)); %identifies which
elements of the array are NaNs
```

```
                                        %and converts the logical
array into and an array
                                        %of double precision values
    VC1 = double(isnan(BF1_nans(1,j).V)); %identifies which
elements of the array are NaNs and
                                    %converts the logical array into
                        and an array of
                                    %double precision values
    VC2 = double(isnan(BF1_nans(2,j).V)); %identifies which
elements of the array are NaNs and
                                    %converts the logical array into
                               and an array of
                                    %double precision values

    %Find "islands" of zeros, which indicate a misidentified
frame (e.g.
    %picking out a bubble or surface feature)
    AC1=abs(AC1-1); %NaNs are zeros; numbers are ones
    AC1_ind=bwlabel(AC1); %each group of ones gets a numbered
integer
    for i=1:max(AC1_ind)
        groupsize=length(find(AC1_ind==i));
        if groupsize<15 %this means that the data are false (not
the nurdle)
            AC1_ind(AC1_ind==i)=0; %Turn these false values into
zeros
        end
    end
    %Now, wherever AC1_ind has zeros, these are NaNs; integers
are numbers
    AC1_ind(AC1_ind>0)=1; %Make all integers in AC1_ind into ones
    AreaC1 = BF1_nans(1,j).A.*AC1_ind;

    for i= 1:length(AreaC1)
        if  isnan(AreaC1(i)) || AreaC1(i) == 0
            AreaC1(i) = 0;
        else
            break
        end
    end

    for i = length(AreaC1):-1:1
        if isnan(AreaC1(i)) || AreaC1(i) == 0
            AreaC1(i) = 0;
        else
            break
        end
    end

    AC2=abs(AC2-1); %NaNs are zeros; numbers are ones
```

```
    AC2_ind=bwlabel(AC2); %each group of ones gets a numbered
integer
    for i=1:max(AC2_ind)
        groupsize=length(find(AC2_ind==i));
        if groupsize<15 %this means that the data are false (not
the nurdle)
            AC2_ind(AC2_ind==i)=0; %Turn these false values into
zeros
        end
    end
    %Now, wherever AC2_ind has zeros, these are NaNs; integers
are numbers
    AC2_ind(AC2_ind>0)=1; %Make all integers in AC2_ind into ones
    AreaC2 = BF1_nans(2,j).A.*AC2_ind;

    for i= 1:length(AreaC2)
        if  isnan(AreaC2(i)) || AreaC2(i) == 0
            AreaC2(i) = 0;
        else
            break
        end
    end

    for i = length(AreaC2):-1:1
        if isnan(AreaC2(i)) || AreaC2(i) == 0
            AreaC2(i) = 0;
        else
            break
        end
    end

    n = 1;
    for i = 1:length(AreaC1)
        if AreaC1(i)~= 0 && AreaC2(i)~=0
            AreaC1_new(n) = AreaC1(i);
            AreaC2_new(n) = AreaC2(i);
            n = n + 1;
        end
    end

    PC1=abs(PC1-1); %NaNs are zeros; numbers are ones
    PC1_ind=bwlabel(PC1); %each group of ones gets a numbered
integer
    for i=1:max(PC1_ind)
        groupsize=length(find(PC1_ind==i));
        if groupsize<15 %this means that the data are false (not
the nurdle)
            PC1_ind(PC1_ind==i)=0; %Turn these false values into
zeros
        end
```

```
    end
    %Now, wherever PC1_ind has zeros, these are NaNs; integers
are numbers
    PC1_ind(PC1_ind>0)=1; %Make all integers in AC1_ind into ones
    PermC1 = BF1_nans(1,j).P.*PC1_ind;

    for i= 1:length(PermC1)
        if  isnan(PermC1(i)) || PermC1(i) == 0
            PermC1(i) = 0;
        else
            break
        end
    end

    for i = length(PermC1):-1:1
        if isnan(PermC1(i)) || PermC1(i) == 0
            PermC1(i) = 0;
        else
            break
        end
    end

    PC2=abs(PC2-1); %NaNs are zeros; numbers are ones
    PC2_ind=bwlabel(PC2); %each group of ones gets a numbered
integer
    for i=1:max(PC2_ind)
        groupsize=length(find(PC2_ind==i));
        if groupsize<15 %this means that the data are false (not
the nurdle)
            PC2_ind(PC2_ind==i)=0; %Turn these false values into
zeros
        end
    end
    %Now, wherever AC2_ind has zeros, these are NaNs; integers
are numbers
    PC2_ind(PC2_ind>0)=1; %Make all integers in AC2_ind into ones
    PermC2 = BF1_nans(2,j).P.*PC2_ind;

    for i= 1:length(PermC2)
        if  isnan(PermC2(i)) || PermC2(i) == 0
            PermC2(i) = 0;
        else
            break
        end
    end

    for i = length(PermC2):-1:1
        if isnan(PermC2(i)) || PermC2(i) == 0
            PermC2(i) = 0;
        else
```

```
            break
        end
    end

    n = 1;
    for i = 1:length(PermC1)
        if PermC1(i)~= 0 && PermC2(i)~=0
            PermC1_new(n) = PermC1(i);
            PermC2_new(n) = PermC2(i);
            n = n + 1;
        end
    end

    XC1=abs(XC1-1); %NaNs are zeros; numbers are ones
    XC1_ind=bwlabel(XC1); %each group of ones gets a numbered
integer
    for i=1:max(XC1_ind)
        groupsize=length(find(XC1_ind==i));
        if groupsize<15 %this means that the data are false (not
the nurdle)
            XC1_ind(XC1_ind==i)=0; %Turn these false values into
zeros
        end
    end
    %Now, wherever AC1_ind has zeros, these are NaNs; integers
are numbers
    XC1_ind(XC1_ind>0)=1; %Make all integers in XC1_ind into ones
    XPosC1 = BF1_nans(1,j).XPos.*XC1_ind;

    for i= 1:length(XPosC1)
        if  isnan(XPosC1(i)) || XPosC1(i) == 0
            XPosC1(i) = 0;
        else
            break
        end
    end

    for i = length(XPosC1):-1:1
        if isnan(XPosC1(i)) || XPosC1(i) == 0
            XPosC1(i) = 0;
        else
            break
        end
    end

    XC2=abs(XC2-1); %NaNs are zeros; numbers are ones
    XC2_ind=bwlabel(XC2); %each group of ones gets a numbered
integer
    for i=1:max(XC2_ind)
        groupsize=length(find(XC2_ind==i));
```

```
        if groupsize<15 %this means that the data are false (not
the nurdle)
            XC2_ind(XC2_ind==i)=0; %Turn these false values into
zeros
        end
    end
    %Now, wherever AC2_ind has zeros, these are NaNs; integers
are numbers
    XC2_ind(XC2_ind>0)=1; %Make all integers in AC2_ind into ones
    XPosC2 = BF1_nans(2,j).XPos.*XC2_ind;

    for i= 1:length(XPosC2)
        if  isnan(XPosC2(i)) || XPosC2(i) == 0
            XPosC2(i) = 0;
        else
            break
        end
    end

    for i = length(XPosC2):-1:1
        if isnan(XPosC2(i)) || XPosC2(i) == 0
            XPosC2(i) = 0;
        else
            break
        end
    end

    n = 1;
    for i = 1:length(XPosC1)
        if XPosC1(i)~= 0 && XPosC2(i)~=0
            XPosC1_new(n) = XPosC1(i);
            XPosC2_new(n) = XPosC2(i);
            n = n + 1;
        end
    end

    YC1=abs(YC1-1); %NaNs are zeros; numbers are ones
    YC1_ind=bwlabel(YC1); %each group of ones gets a numbered
integer
    for i=1:max(YC1_ind)
        groupsize=length(find(YC1_ind==i));
        if groupsize<15 %this means that the data are false (not
the nurdle)
            YC1_ind(YC1_ind==i)=0; %Turn these false values into
zeros
        end
    end
    %Now, wherever AC1_ind has zeros, these are NaNs; integers
are numbers
    YC1_ind(YC1_ind>0)=1; %Make all integers in YC1_ind into ones
```

```
    YPosC1 = BF1_nans(1,j).YPos.*YC1_ind;

    for i= 1:length(YPosC1)
        if  isnan(YPosC1(i)) || YPosC1(i) == 0
            YPosC1(i) = 0;
        else
            break
        end
    end

    for i = length(YPosC1):-1:1
        if isnan(YPosC1(i)) || YPosC1(i) == 0
            YPosC1(i) = 0;
        else
            break
        end
    end

    YC2=abs(YC2-1); %NaNs are zeros; numbers are ones
    YC2_ind=bwlabel(YC2); %each group of ones gets a numbered
integer
    for i=1:max(YC2_ind)
        groupsize=length(find(YC2_ind==i));
        if groupsize<15 %this means that the data are false (not
the nurdle)
            YC2_ind(YC2_ind==i)=0; %Turn these false values into
zeros
        end
    end
    %Now, wherever YC2_ind has zeros, these are NaNs; integers
are numbers
    YC2_ind(YC2_ind>0)=1; %Make all integers in AC2_ind into ones
    YPosC2 = BF1_nans(2,j).YPos.*YC2_ind;

    for i= 1:length(YPosC2)
        if  isnan(YPosC2(i)) || YPosC2(i) == 0
            YPosC2(i) = 0;
        else
            break
        end
    end

    for i = length(YPosC2):-1:1
        if isnan(YPosC2(i)) || YPosC2(i) == 0
            YPosC2(i) = 0;
        else
            break
        end
    end
```

```
    n = 1;
    for i = 1:length(YPosC1)
        if YPosC1(i)~= 0 && YPosC2(i)~=0
            YPosC1_new(n) = YPosC1(i);
            YPosC2_new(n) = YPosC2(i);
            n = n + 1;
        end
    end

    VC1=abs(VC1-1); %NaNs are zeros; numbers are ones
    VC1_ind=bwlabel(VC1); %each group of ones gets a numbered
integer
    for i=1:max(VC1_ind)
        groupsize=length(find(VC1_ind==i));
        if groupsize<15 %this means that the data are false (not
the nurdle)
            VC1_ind(VC1_ind==i)=0; %Turn these false values into
zeros
        end
    end
    %Now, wherever AC1_ind has zeros, these are NaNs; integers
are numbers
    VC1_ind(VC1_ind>0)=1; %Make all integers in VC1_ind into ones
    VelC1 = BF1_nans(1,j).V.*VC1_ind;

    for i= 1:length(VelC1)
        if  isnan(VelC1(i)) || VelC1(i) == 0
            VelC1(i) = 0;
        else
            break
        end
    end

    for i = length(VelC1):-1:1
        if isnan(VelC1(i)) || VelC1(i) == 0
            VelC1(i) = 0;
        else
            break
        end
    end

    VC2=abs(VC2-1); %NaNs are zeros; numbers are ones
    VC2_ind=bwlabel(VC2); %each group of ones gets a numbered
integer
    for i=1:max(VC2_ind)
        groupsize=length(find(VC2_ind==i));
        if groupsize<15 %this means that the data are false (not
the nurdle)
            VC2_ind(VC2_ind==i)=0; %Turn these false values into
zeros
```

```
        end
    end
    %Now, wherever AC2_ind has zeros, these are NaNs; integers
are numbers
    VC2_ind(VC2_ind>0)=1; %Make all integers in AC2_ind into ones
    VelC2 = BF1_nans(2,j).V.*VC2_ind;

    for i= 1:length(VelC2)
        if  isnan(VelC2(i)) || VelC2(i) == 0
            VelC2(i) = 0;
        else
            break
        end
    end

    for i = length(VelC2):-1:1
        if isnan(VelC2(i)) || VelC2(i) == 0
            VelC2(i) = 0;
        else
            break
        end
    end

    n = 1;
    for i = 1:length(VelC1)
        if VelC1(i)~= 0 && VelC2(i)~=0
            VelC1_new(n) = VelC1(i);
            VelC2_new(n) = VelC2(i);
            n = n + 1;
        end
    end

    %Save the data in a new Data Structure to its correct
parameter
    BF1(1,j).A = AreaC1_new;
    BF1(2,j).A = AreaC2_new;
    BF1(1,j).P = PermC1_new;
    BF1(2,j).P = PermC2_new;
    BF1(1,j).XPos = XPosC1_new;
    BF1(2,j).XPos = XPosC2_new;
    BF1(1,j).YPos = YPosC1_new;
    BF1(2,j).YPos = YPosC2_new;
    BF1(1,j).V = VelC1_new;
    BF1(2,j).V = VelC2_new;

    save('BF1.mat','BF1','-v7.3')
end
```

Appendix C

The following tables show the variability in the 5 trials for one nurdle compared to the overall variability across all 50 nurdles in each treatment group. They show the mean standard deviation across 5 nurdles compared to the standard deviation of the mean rise velocity across all 50 nurdles. These data indicate that there was not large amount variability from test-to-test with the same nurdle and that the average of the five videos for each nurdle is representative of the overall behavior of the individual nurdle.

BF1 Treatment Group Camera #1	**Mean rise velocity across five trials**	**Standard deviation of rise velocity across five trials**
Nurdle #01	5.56	0.21
Nurdle #02	5.21	0.24
Nurdle #03	4.10	0.35
Nurdle #04	4.84	0.26
Nurdle #05	5.11	0.30
Nurdle #06	4.66	0.84
Nurdle #07	5.77	0.80
Nurdle #08	4.40	0.25
Nurdle #09	4.70	0.12
Nurdle #10	6.17	0.10
Nurdle #11	3.06	0.07
Nurdle #12	4.59	0.14
Nurdle #13	4.64	0.10
Nurdle #14	5.74	0.10
Nurdle #15	6.36	0.17
Nurdle #16	3.43	0.09
Nurdle #17	4.59	0.04
Nurdle #18	3.84	0.10
Nurdle #19	4.85	0.28
Nurdle #20	5.25	0.39
Nurdle #21	4.53	0.20
Nurdle #22	4.74	0.17
Nurdle #23	5.50	0.14
Nurdle #24	4.43	0.25
Nurdle #25	5.20	0.11
Nurdle #26	4.79	0.32

Nurdle #27	4.66	0.14
Nurdle #28	3.77	0.13
Nurdle #29	4.51	0.21
Nurdle #30	5.84	0.25
Nurdle #31	5.67	0.06
Nurdle #32	5.05	0.25
Nurdle #33	5.64	0.25
Nurdle #34	4.69	0.21
Nurdle #35	5.12	0.75
Nurdle #36	3.88	0.06
Nurdle #37	5.63	0.31
Nurdle #38	4.92	0.17
Nurdle #39	4.52	0.26
Nurdle #40	4.35	0.16
Nurdle #41	3.90	0.09
Nurdle #42	5.09	0.13
Nurdle #43	5.33	0.10
Nurdle #44	5.36	0.26
Nurdle #45	5.36	0.05
Nurdle #46	4.81	0.21
Nurdle #47	4.26	0.07
Nurdle #48	5.35	0.61
Nurdle #49	4.65	0.07
Nurdle #50	4.20	0.03
mean rise velocity standard deviation per nurdle:		**0.22**
standard deviation of mean rise velocity across all nurdles:		**0.69**

BF1 Treatment Group Camera #2	**Mean rise velocity across five trials**	**Standard deviation of rise velocity across five trials**
Nurdle #01	5.45	0.18
Nurdle #02	5.13	0.15
Nurdle #03	4.06	0.31
Nurdle #04	4.67	0.25
Nurdle #05	4.94	0.36
Nurdle #06	4.50	0.77
Nurdle #07	5.60	0.73
Nurdle #08	4.29	0.28
Nurdle #09	4.54	0.17
Nurdle #10	6.22	0.13

Nurdle #11	2.99	0.09
Nurdle #12	4.55	0.13
Nurdle #13	4.60	0.14
Nurdle #14	5.76	0.16
Nurdle #15	6.28	0.38
Nurdle #16	3.40	0.08
Nurdle #17	4.64	0.10
Nurdle #18	3.85	0.17
Nurdle #19	4.78	0.26
Nurdle #20	5.24	0.27
Nurdle #21	4.51	0.18
Nurdle #22	4.73	0.16
Nurdle #23	5.41	0.09
Nurdle #24	4.30	0.22
Nurdle #25	5.19	0.06
Nurdle #26	4.92	0.31
Nurdle #27	4.80	0.04
Nurdle #28	3.84	0.13
Nurdle #29	4.67	0.25
Nurdle #30	6.02	0.25
Nurdle #31	5.83	0.07
Nurdle #32	5.29	0.25
Nurdle #33	5.82	0.22
Nurdle #34	4.82	0.17
Nurdle #35	5.32	0.76
Nurdle #36	3.98	0.08
Nurdle #37	5.87	0.25
Nurdle #38	4.89	0.15
Nurdle #39	4.46	0.26
Nurdle #40	4.27	0.15
Nurdle #41	3.92	0.09
Nurdle #42	4.99	0.12
Nurdle #43	5.23	0.08
Nurdle #44	5.28	0.23
Nurdle #45	5.30	0.06
Nurdle #46	4.75	0.14
Nurdle #47	4.24	0.08
Nurdle #48	5.24	0.58
Nurdle #49	4.60	0.11
Nurdle #50	4.17	0.07

mean rise velocity standard deviation per nurdle:	**0.21**
standard deviation of mean rise velocity across all nurdles:	**0.70**

N1 Treatment Group Camera #1	Mean rise velocity across five trials	Standard deviation of rise velocity across five trials
Nurdle #01	6.05	0.31
Nurdle #02	5.92	0.28
Nurdle #03	6.68	0.25
Nurdle #04	5.84	0.25
Nurdle #05	6.05	0.31
Nurdle #06	4.61	0.22
Nurdle #07	5.62	0.25
Nurdle #08	4.96	0.16
Nurdle #09	5.33	0.23
Nurdle #10	6.69	0.22
Nurdle #11	3.24	0.29
Nurdle #12	5.52	0.24
Nurdle #13	5.14	0.40
Nurdle #14	5.38	0.26
Nurdle #15	6.84	0.25
Nurdle #16	3.88	0.27
Nurdle #17	5.13	0.19
Nurdle #18	4.79	0.22
Nurdle #19	5.38	0.29
Nurdle #20	5.96	0.26
Nurdle #21	5.45	0.26
Nurdle #22	5.65	0.25
Nurdle #23	6.13	0.34
Nurdle #24	5.32	0.23
Nurdle #25	5.87	0.26
Nurdle #26	5.36	0.23
Nurdle #27	5.19	0.21
Nurdle #28	4.48	0.43
Nurdle #29	5.08	0.19
Nurdle #30	6.24	0.24
Nurdle #31	5.69	0.24
Nurdle #32	5.67	0.23
Nurdle #33	6.53	0.23
Nurdle #34	5.05	0.20

Nurdle #35	6.02	0.24
Nurdle #36	4.07	0.22
Nurdle #37	6.06	0.28
Nurdle #38	5.53	0.26
Nurdle #39	6.13	0.20
Nurdle #40	5.24	0.23
Nurdle #41	4.21	0.21
Nurdle #42	6.04	0.25
Nurdle #43	5.48	0.45
Nurdle #44	6.19	0.24
Nurdle #45	6.77	0.24
Nurdle #46	6.32	0.25
Nurdle #47	4.86	0.31
Nurdle #48	6.36	0.53
Nurdle #49	5.41	0.22
Nurdle #50	4.63	0.17
mean rise velocity standard deviation per nurdle:		**0.26**
standard deviation of mean rise velocity across all nurdles:		**0.77**

N1 Treatment Group Camera #2	Mean rise velocity across five trials	Standard deviation of rise velocity across five trials
Nurdle #1	5.92	0.11
Nurdle #2	5.84	0.06
Nurdle #3	6.57	0.13
Nurdle #4	5.75	0.09
Nurdle #5	5.94	0.11
Nurdle #6	4.65	0.40
Nurdle #7	5.49	0.13
Nurdle #8	4.96	0.17
Nurdle #9	5.20	0.07
Nurdle #10	6.61	0.29
Nurdle #11	3.24	0.16
Nurdle #12	5.43	0.57
Nurdle #13	5.05	0.07
Nurdle #14	5.31	0.48
Nurdle #15	6.89	0.18
Nurdle #16	3.86	0.15
Nurdle #17	5.13	0.14
Nurdle #18	4.76	0.19

Nurdle #19	5.29	0.22
Nurdle #20	5.91	0.09
Nurdle #21	5.28	0.25
Nurdle #22	5.62	0.13
Nurdle #23	6.15	0.75
Nurdle #24	5.48	0.50
Nurdle #25	5.80	0.13
Nurdle #26	5.41	0.04
Nurdle #27	5.08	0.05
Nurdle #28	4.42	0.08
Nurdle #29	5.01	0.09
Nurdle #30	6.20	0.21
Nurdle #31	5.64	0.09
Nurdle #32	5.60	0.15
Nurdle #33	6.54	0.22
Nurdle #34	5.06	0.13
Nurdle #35	6.02	0.30
Nurdle #36	4.04	0.08
Nurdle #37	6.13	0.18
Nurdle #38	5.71	0.44
Nurdle #39	6.07	0.07
Nurdle #40	5.23	0.37
Nurdle #41	4.25	0.07
Nurdle #42	6.12	0.15
Nurdle #43	5.52	0.14
Nurdle #44	6.14	0.34
Nurdle #45	6.78	0.05
Nurdle #46	6.30	0.34
Nurdle #47	4.86	0.13
Nurdle #48	6.34	0.12
Nurdle #49	5.48	0.32
Nurdle #50	4.60	0.20
mean rise velocity standard deviation per nurdle:		**0.20**
standard deviation of mean rise velocity across all nurdles:		**0.77**

BF2 Treatment Group Camera #1	**Mean rise velocity across five trials**	**Standard deviation of rise velocity across five trials**
Nurdle #01	5.58	0.09
Nurdle #02	5.82	0.15

Nurdle #03	5.59	0.12
Nurdle #04	5.68	0.22
Nurdle #05	7.05	0.11
Nurdle #06	5.31	0.14
Nurdle #07	5.71	0.20
Nurdle #08	5.77	0.06
Nurdle #09	4.36	0.08
Nurdle #10	4.50	0.09
Nurdle #11	5.41	0.09
Nurdle #12	4.74	0.09
Nurdle #13	4.75	0.03
Nurdle #14	5.67	0.22
Nurdle #15	4.97	0.13
Nurdle #16	4.57	0.07
Nurdle #17	4.73	0.14
Nurdle #18	6.44	0.33
Nurdle #19	4.66	0.08
Nurdle #20	5.46	0.21
Nurdle #21	5.52	0.27
Nurdle #22	5.43	0.26
Nurdle #23	5.67	0.09
Nurdle #24	4.68	0.13
Nurdle #25	6.10	0.11
Nurdle #26	4.25	0.24
Nurdle #27	5.15	0.04
Nurdle #28	6.17	0.05
Nurdle #29	3.76	0.22
Nurdle #30	3.76	0.11
Nurdle #31	6.15	0.15
Nurdle #32	5.62	0.16
Nurdle #33	4.67	0.08
Nurdle #34	5.45	0.17
Nurdle #35	4.61	0.14
Nurdle #36	4.31	0.13
Nurdle #37	5.53	0.06
Nurdle #38	6.05	0.19
Nurdle #39	5.09	0.19
Nurdle #40	4.91	0.11
Nurdle #41	3.90	0.06
Nurdle #42	5.71	0.21

Nurdle #43	5.67	0.13
Nurdle #44	5.15	0.12
Nurdle #45	6.12	0.19
Nurdle #46	6.61	0.06
Nurdle #47	5.88	0.25
Nurdle #48	7.06	0.20
Nurdle #49	6.28	0.16
Nurdle #50	6.52	0.19
mean rise velocity standard deviation per nurdle:		**0.14**
standard deviation of mean rise velocity across all nurdles:		**0.79**

BF2 Treatment Group Camera #1	Mean rise velocity across five trials	Standard deviation of rise velocity across five trials
Nurdle #01	5.55	0.22
Nurdle #02	5.72	0.12
Nurdle #03	5.42	0.16
Nurdle #04	5.62	0.22
Nurdle #05	6.85	0.16
Nurdle #06	5.27	0.11
Nurdle #07	5.65	0.19
Nurdle #08	5.73	0.17
Nurdle #09	4.33	0.03
Nurdle #10	4.40	0.05
Nurdle #11	5.28	0.12
Nurdle #12	4.62	0.11
Nurdle #13	4.69	0.10
Nurdle #14	5.52	0.22
Nurdle #15	4.95	0.13
Nurdle #16	4.42	0.15
Nurdle #17	4.68	0.25
Nurdle #18	6.51	0.44
Nurdle #19	4.59	0.12
Nurdle #20	5.37	0.22
Nurdle #21	5.46	0.24
Nurdle #22	5.43	0.16
Nurdle #23	5.69	0.08
Nurdle #24	4.64	0.10
Nurdle #25	6.02	0.10
Nurdle #26	4.24	0.15

Nurdle #27	5.20	0.16
Nurdle #28	6.15	0.14
Nurdle #29	3.74	0.17
Nurdle #30	3.84	0.14
Nurdle #31	6.10	0.18
Nurdle #32	5.59	0.18
Nurdle #33	4.73	0.13
Nurdle #34	5.45	0.09
Nurdle #35	4.66	0.09
Nurdle #36	4.33	0.12
Nurdle #37	5.50	0.15
Nurdle #38	6.08	0.20
Nurdle #39	5.04	0.19
Nurdle #40	4.89	0.09
Nurdle #41	3.92	0.05
Nurdle #42	5.73	0.16
Nurdle #43	5.63	0.14
Nurdle #44	5.16	0.06
Nurdle #45	6.10	0.18
Nurdle #46	6.54	0.17
Nurdle #47	5.93	0.25
Nurdle #48	7.08	0.15
Nurdle #49	6.33	0.18
Nurdle #50	6.40	0.19
mean rise velocity standard deviation per nurdle:		**0.15**
standard deviation of mean rise velocity across all nurdles:		**0.78**

N2 Treatment Group Camera #1	**Mean rise velocity across five trials**	**Standard deviation of rise velocity across five trials**
Nurdle #01	5.57	0.13
Nurdle #02	5.89	0.09
Nurdle #03	5.59	0.09
Nurdle #04	5.77	0.30
Nurdle #05	6.89	0.20
Nurdle #06	5.41	0.15
Nurdle #07	5.46	0.13
Nurdle #08	5.00	0.98
Nurdle #09	5.71	0.33
Nurdle #10	5.29	0.19

Nurdle #11	5.44	0.12
Nurdle #12	4.77	0.19
Nurdle #13	4.67	0.14
Nurdle #14	5.80	0.33
Nurdle #15	4.96	0.17
Nurdle #16	4.49	0.12
Nurdle #17	4.66	0.09
Nurdle #18	6.59	0.38
Nurdle #19	4.73	0.11
Nurdle #20	5.36	0.17
Nurdle #21	5.35	0.23
Nurdle #22	5.65	0.09
Nurdle #23	5.82	0.18
Nurdle #24	5.88	0.32
Nurdle #25	6.38	0.18
Nurdle #26	4.92	0.46
Nurdle #27	5.30	0.10
Nurdle #28	6.60	0.42
Nurdle #29	3.88	0.10
Nurdle #30	5.64	0.27
Nurdle #31	6.39	0.09
Nurdle #32	5.82	0.15
Nurdle #33	6.18	0.07
Nurdle #34	5.66	0.23
Nurdle #35	5.31	0.13
Nurdle #36	5.24	0.06
Nurdle #37	5.87	0.12
Nurdle #38	5.97	0.27
Nurdle #39	5.24	0.60
Nurdle #40	5.17	0.33
Nurdle #41	5.90	0.10
Nurdle #42	5.79	0.09
Nurdle #43	5.55	0.22
Nurdle #44	5.33	0.20
Nurdle #45	6.47	0.09
Nurdle #46	6.44	0.16
Nurdle #47	6.11	0.05
Nurdle #48	7.18	0.12
Nurdle #49	6.53	0.09
Nurdle #50	6.63	0.13

mean rise velocity standard deviation per nurdle:	**0.20**
standard deviation of mean rise velocity across all nurdles:	**0.66**

N2 Treatment Group Camera #1	Mean rise velocity across five trials	Standard deviation of rise velocity across five trials
Nurdle #01	5.50	0.08
Nurdle #02	5.74	0.11
Nurdle #03	5.50	0.11
Nurdle #04	5.69	0.26
Nurdle #05	6.83	0.19
Nurdle #06	5.37	0.15
Nurdle #07	5.43	0.19
Nurdle #08	4.92	0.92
Nurdle #09	5.65	0.28
Nurdle #10	5.20	0.13
Nurdle #11	5.40	0.09
Nurdle #12	4.73	0.14
Nurdle #13	4.65	0.12
Nurdle #14	5.75	0.34
Nurdle #15	4.94	0.19
Nurdle #16	4.51	0.03
Nurdle #17	4.62	0.11
Nurdle #18	6.59	0.37
Nurdle #19	4.66	0.19
Nurdle #20	5.33	0.15
Nurdle #21	5.34	0.30
Nurdle #22	5.65	0.07
Nurdle #23	5.83	0.20
Nurdle #24	5.89	0.28
Nurdle #25	6.34	0.11
Nurdle #26	4.92	0.43
Nurdle #27	5.37	0.20
Nurdle #28	6.58	0.42
Nurdle #29	3.91	0.06
Nurdle #30	5.62	0.28
Nurdle #31	6.37	0.07
Nurdle #32	5.84	0.14
Nurdle #33	6.13	0.08
Nurdle #34	5.66	0.31

Nurdle #35	5.35	0.26
Nurdle #36	5.27	0.09
Nurdle #37	5.84	0.17
Nurdle #38	6.05	0.27
Nurdle #39	5.26	0.57
Nurdle #40	5.18	0.31
Nurdle #41	5.81	0.17
Nurdle #42	5.77	0.09
Nurdle #43	5.64	0.26
Nurdle #44	5.42	0.30
Nurdle #45	6.46	0.04
Nurdle #46	6.48	0.09
Nurdle #47	6.15	0.06
Nurdle #48	7.25	0.14
Nurdle #49	6.47	0.10
Nurdle #50	6.60	0.17
mean rise velocity standard deviation per nurdle:		**0.20**
standard deviation of mean rise velocity across all nurdles:		**0.66**